

Lake volume and potential hazards of moraine-dammed glacial lakes in temperature glaciation regions—A case study of Bienong Co

Hongyu Duan¹, Xiaojun Yao¹, Yuan Zhang¹, Huian Jin², Qi Wang³, Zhishui Du³, Jiayu Hu¹, Bin Wang⁴, and Qianxun Wang⁵

¹ College of Geography and Environment Science, Northwest Normal University, Lanzhou, 730070, China

² Gansu Forestry Polytechnic, Tianshui, 741020, China

³ Northwest Engineering Corporation Limited, Power China, Xi'an 710065, China

⁴ Xinjiang Transport Planning Survey and Design Institute Company Limited, Urumqi 830006, China

⁵ Capital Urban Planning and Design Consulting Development Company Limited, Beijing 100038, China

Correspondence to: Xiaojun Yao (xj_yao@nwnu.edu.cn)

Abstract. The existence of glacial lakes in the Southeastern Tibetan Plateau (SETP) is a potential hazard to downstream regions, as the outburst of such lakes has the potential to result in disastrous glacial lake outburst floods (GLOFs). In the present study, we conducted a comprehensive investigation for Bienong Co, a moraine-dammed glacial lake in the SETP. First, the lake basin morphology was determined and the lake volume was estimated, showing that the maximum lake depth is ~181 m and the lake volume is $\sim 102.3 \times 10^6 \text{ m}^3$. Then, we analysed scenarios for possible lake outbursts. These scenarios included the possibility of GLOFs being triggered by the ice avalanches (Scenarios A1-3) or the lateral moraines landslides entering the lake (Scenarios B1-3 and C1-3). We assumed that the ice avalanche (Scenarios A1, A2, and A3) and the lateral moraine landslide (Scenarios B1, B2, and B3 and C1, C2, and C3) induced GLOFs process chain of Bienong Co. The avalanche volumes of the nine trigger scenarios were obtained calculated using the from the RAMMS modeling results, and Next, the displacement wave the BASEMENT model was used to simulate the generation and propagation of the avalanche-induced displacement waves in the lake. With the BASEMENT model, the overtopping flow and erosion on the moraine dam and the subsequent downstream flooding were also simulated. The results demonstrate indicate that the ice avalanche scenarios produce may cause the largest amount of material entering into the lake, resulting in a displacement wave amplitudes of up to 25.2 m in amplitude (Scenario A3) near the moraine dam. Smaller volumes of landslides volumes entering the lake only result in smaller displacement waves in the lake, such as for example, that Scenario C1 has a wave amplitude below 1 m near the moraine dam. Scenarios A1, A2, and A3 result in released water volumes from the lake of $24.1 \times 10^6 \text{ m}^3$, $25.3 \times 10^6 \text{ m}^3$, and $26.4 \times 10^6 \text{ m}^3$. Corresponding, and peak discharges at the moraine dam of are 4,996 m^3/s , 7,817 m^3/s , and 13,078 m^3/s , respectively. These high discharges cause scour erosion of the moraine dams, resulting in breach widths of 295.0 m, 339.4 m, and 368.5 m, respectively, with the generally similar breach depth of approximately 19 m. and breach depths of 19.0 m, 19.1 m, 19.3 m, respectively. However, in landslide scenarios, only the overtopping flow generated by Scenarios B3 and C3 caused moderate erosion of the moraine dam, with breach depths of 6.5 m and 7.9 m, and breach widths of 153 m and 169 m, respectively. According to our simulations, GLOFs generated by Scenario A1, A2, and A3 can all flow through 18 settlements downstream within 20 h, thereby threatening and will threaten more than half of the settlements. Both Scenarios B3 and C3 produced GLOFs floods that flow through eight downstream settlements within 20 h and had have a relatively small impact on them. Comparisons of area, depth and volume of glacier lakes show that Bienong Co is the relative-known deepest glacial lake known on the Tibetan Plateau in the same surface area. This study could provide new insight about moraine-dammed glacial lakes in the SETP and a valuable reference for GLOFs disaster prevention for local governments.

1 Introduction

Due to global warming, accelerated retreat and thinning of glaciers has occurred in most regions compared to the last century (Zemp et al., 2019), resulting in a rapid increase in the number, area, and volume of glacial lakes worldwide (Shugar et al., 2020; Wang et al., 2020). Glacier meltwater can be confined and stored in certain depressions dammed by moraine, ice, or bedrock (Vilímek et al., 2013). Once the dam is damaged, the water can be suddenly ~~and catastrophically~~ released to form glacial lake outburst floods (GLOFs), which ~~could have a significant downstream~~ ~~may cause severe~~ social and geomorphic impacts ~~across~~ several dozens of kilometers ~~and more downstream~~ (Lliboutry, 1977; Richardson and Reynolds, 2000; Osti and Egashira, 2009; Carrivick and Tweed, 2016; Cook et al., 2018; Harrison et al., 2018; Zheng et al., 2021). Moraine-dammed glacial lakes are of particular concern due to their large volume (Fujita et al., 2013; Veh et al., 2019), weak dam composition, and exposure to various triggers, such as ice ~~and~~ or rock avalanches, heavy precipitation, and intense glacier ~~melting~~ ~~meltwater~~ (Emmer and Cochachin, 2013; Nie et al., 2018), ~~which are the most common sources of GLOFs (Watanabe and Rothacher, 1996; Westoby et al., 2014).~~ The Himalayas and the Southeastern Tibetan Plateau (SETP) are regions of ~~the~~ frequent ~~occurrence of~~ GLOFs caused by moraine-dammed glacial lakes (Wang, 2016). Veh et al. (2019) deemed that the Himalayas, particularly the southern region, would likely experience more GLOFs in the coming decades. Research shows that the Himalayas, especially the southern region, are likely to experience more GLOFs in the coming decades (Veh et al., 2019).

The SETP is a broad mountainous ~~area~~ region with highly complicated terrains, including covering the central and eastern Nyainqêntanglha Ranges, ~~the~~ eastern Himalayas, and ~~the~~ western Hengduan Mountains, ~~and has highly complicated terrains~~ (Ke et al., 2014). ~~Controlled by warm and humid Indian monsoons, a~~ A substantial large number of temperate glaciers have developed here under the influence of the warm and humid Indian monsoons (Yang et al., 2008), with characteristics such as ~~featured as~~ adequate recharge, ~~strong~~ intense ablation, low snowline distribution, high temperature, fast movement, and strong ~~geological, as well as~~ geomorphological, effect (Li et al., 1986; Qin et al., 2012; Liu et al., 2014). In the past decades, glaciers in this region have undergone significant negative mass balances ~~which have been observed with markedly negative mass balances during the past decades~~ (Kääb et al., 2012; Neckel et al., 2014; Kääb et al., 2015; Brun et al., 2017; Dehecq et al., 2019). Therefore, the combination of active glacial processes and heavy rainfall during the monsoon season makes the region prone to glacier-related natural hazards (Wang et al., 2012a). Studies of glacial lakes in the SETP have mainly focused on the regional-scale assessments of glacial lake changes (Wang et al., 2011b; Song et al., 2016; Wang et al., 2017; Zhang et al., 2020; Zhang et al., 2021), identification of potentially dangerous glacial lakes (Wang et al., 2011a; Liu et al., 2019; Duan et al., 2020; Qi et al., 2020), site-specific analysis of formation mechanisms, development trends, risk evolution and management measures of GLOFs (Cui et al., 2003; Cheng et al., 2008, 2009; Sun et al., 2014; Liu et al., 2021; Wang et al., 2021), and exploration of geological features of a single glacial lake (Yuan et al., 2012; Liu et al., 2015; Huang et al., 2016). Fewer studies have applied hydrodynamic models to simulate GLOFs in the SETP. Wang et al. (2011b) evaluated the applicability of ASTER GDEM (the Global Digital Elevation Model) and SRTM DEM in the simulation of GLOF processes based on the HEC-RAS hydrodynamic model (Brunner, 2002). Zheng et al. (2021) analyzed and reconstructed a GLOF process chain of Jinwu Co using published empirical relationships and the GIS-based r.avaflow simulation tool (Mergili et al., 2017; Pudasaini and Mergili, 2019; Mergili and Pudasaini, 2020).

As a key factor related to the peak discharge and outburst volume of a GLOF event (Evans, 1987; Huggel et al., 2002), lake volume is difficult to ~~directly~~ obtain ~~by means of~~ using a satellite remote sensing approach directly. Currently, ~~due to the easy availability of area information from remote sensing images,~~ the volume of a glacial lakes is generally estimated using ~~the developed~~ empirical formulas and the its area information from remote sensing images. Empirical formulas linking the areas and volumes of glacial lakes were generally developed based on the bathymetry data of a small number of glacial lakes to connect glacial lake area and volume based on bathymetric data for a small number of glacial lakes (O'Connor et al., 2001; Huggel et al., 2002; Yao et al., 2014). ~~However,~~ the estimated volume may be inaccurate because of the unique geographical conditions of different glacial lakes (Cook and Quincey, 2015). Despite the high prevalence of GLOFs in ~~Although~~ the SETP region ~~is an area with a high incidence of GLOFs~~ (Sun et al., 2014; Zheng et al., 2021; Zhang et al., 2023), there are ~~have been~~

few publicly available bathymetric bathymetry data of on glacial lakes and related research works. The Previous previous bathymetric works in the Tibetan Plateau were carried out mainly for glacial lakes located in the Himalayas (LIGG/WECS/NEA, 1988; Geological Survey of India, 1995; Yamada, 1998; Mool et al., 2001; Sakai, 2003; Yamada, 2004; ICIMOD, 2011; Sakai, 2012; Yao et al., 2012; Wang et al., 2015; Haritashya et al., 2018; Sharma et al., 2018; Li et al., 2021).

85 This It is unfavorable to fully understand the morphology and optimal disaster prevention strategies of glacial lakes in the SETP region. In recent years, unmanned surface vessels (USVs) have developed rapidly (Liu et al., 2016), and have been widely used in specific certain scenarios, such as bathymetric map creation, transportation, environmental monitoring, and moraine marine surveys (Larrazabal and Peñas, 2016; Yan et al., 2010; Specht et al., 2019), owing to personnel safety and high flexibility in complex environments. Glacial lakes are mainmostly located at high altitudes and in harsh environments (Zhang et al., 2020), a The application of USVs makes the underwater topography measurement of glacial lakes more accurate, efficient, and safer and USVs make the measurement of the underwater topography of glacial lakes safer, more convenient, and more accurate (Li et al., 2021).

In this study, we aim to complete an investigation of the potential GLOF hazard of an end moraine-dammed glacial lake, Bienong Co (“Co” means “lake” in Tibetan) in the SETP based on field bathymetric data and remote sensing data using a multi-model combination method. First, we determined the lake basin morphology of Bienong Co is modelled. Then, we simulated the multiple components of the GLOF process chain, including starting with the initial mass movement from the mother glacier and the lateral moraines slope, displacement wave the generation and propagation of displacement waves in the lake, the overtopping flow and erosion on the moraine dam, and the subsequent downstream flooding were simulated. This study will assist the local government into understanding the potential hazards of Bienong Co and serve as a reference for other scholars studying glacial lakes and GLOFs in the SETP region.

2 Study area

Bienong Co is located in the upper area region of the Yi’ong Zangbo (“Zangbo” means “river” in Tibetan) watershed basin (30°05' - 31°03'N, 92°52' - 95°19'E) in the SETP (Fig. 1a). As a one-level tributary of the Parlung Zangbo and a two-level tributary of the Yarlung Zangbo (i.e., the Brahmaputra River), the Yi’ong Zangbo drains an area covering 13,533 km². With tall mountains and deep valleys, The the terrain is high in the west and low in the east with high mountains and valleys. The region experiences a climate is warm and humid climate with, featuring a mean annual precipitation of 958 mm and a mean annual temperature of 8.8 °C (Ke et al., 2013, 2014). In 2016, There there was were 1,907.76 km² glacier coverage, and 105 moraine-dammed glacial lakes with a total area of 16.87 km² in the Yi’ong Zangbo basin, in 2016 (Duan et al., 2020). Seven glacial lakes in the basin watershed, including Bienong Co, were considered to have high GLOFs potential (Duan et al., 110 2020), of which Jinwu Co collapsed failed on June 26, 2020 (Zheng et al., 2021). Three catastrophic GLOFs have occurred in the Yi’ong Zangbo basin As as of 2021, there have been three recorded large GLOF events in the basin, all of which caused very significantly damaged to infrastructures in the downstream region (Sun et al., 2014; Yao et al., 2014; Zheng et al., 2021) (Fig. 1b). Bienong Co is an end moraine-dammed lake constrained by the mother glacier (Mulang Glacier) on the south and a massive unconsolidated terminal moraine dam on the northwest (Fig. 1c). In 2021, it had an area of 1.15 ± 0.05 km² and a surface elevation of 4,745 m The elevation of the water surface in 2021 was 4,745 m covering an area of 1.15 ± 0.05 km² that has experienced less significant changes. The Mulang Glacier, which has remained stable in size over the past 45 years, had an area of 8.29 ± 0.22 km² and with a mean surface slope of ~18.28°, which has also remained a largely unchanged area over the last 45 years. However, the The glacier ablation zone, however, underwent an intense thinning at a speed of -6.5 m/a experienced a thinning process of 6.5 m/a. One of the major tributaries of the upper Yi’ong Zangbo, The flow of Bienong Co converges into Xiong Qu (“Qu” means “river” in Tibetan), receives the flow from Bienong Co which is one of the two main tributaries of the upper Yi’ong Zangbo (Fig. 1b). The flow channel from Bienong Co to the confluence of Xiong Qu and Song

Qu (another major tributary of the upper Yi'ong Zangbo) stretches ~53 km long, with a river-longitudinal drop ratio of 14.48%. There are 18 settlements, and 13 bridges, and a substantial amount of cultivated land densely distributed along the flow channel, as well as a large amount of agricultural land. In a additionally, the Jiazhong Highway extends closely adjacent to along the river (Fig. 1d).

125

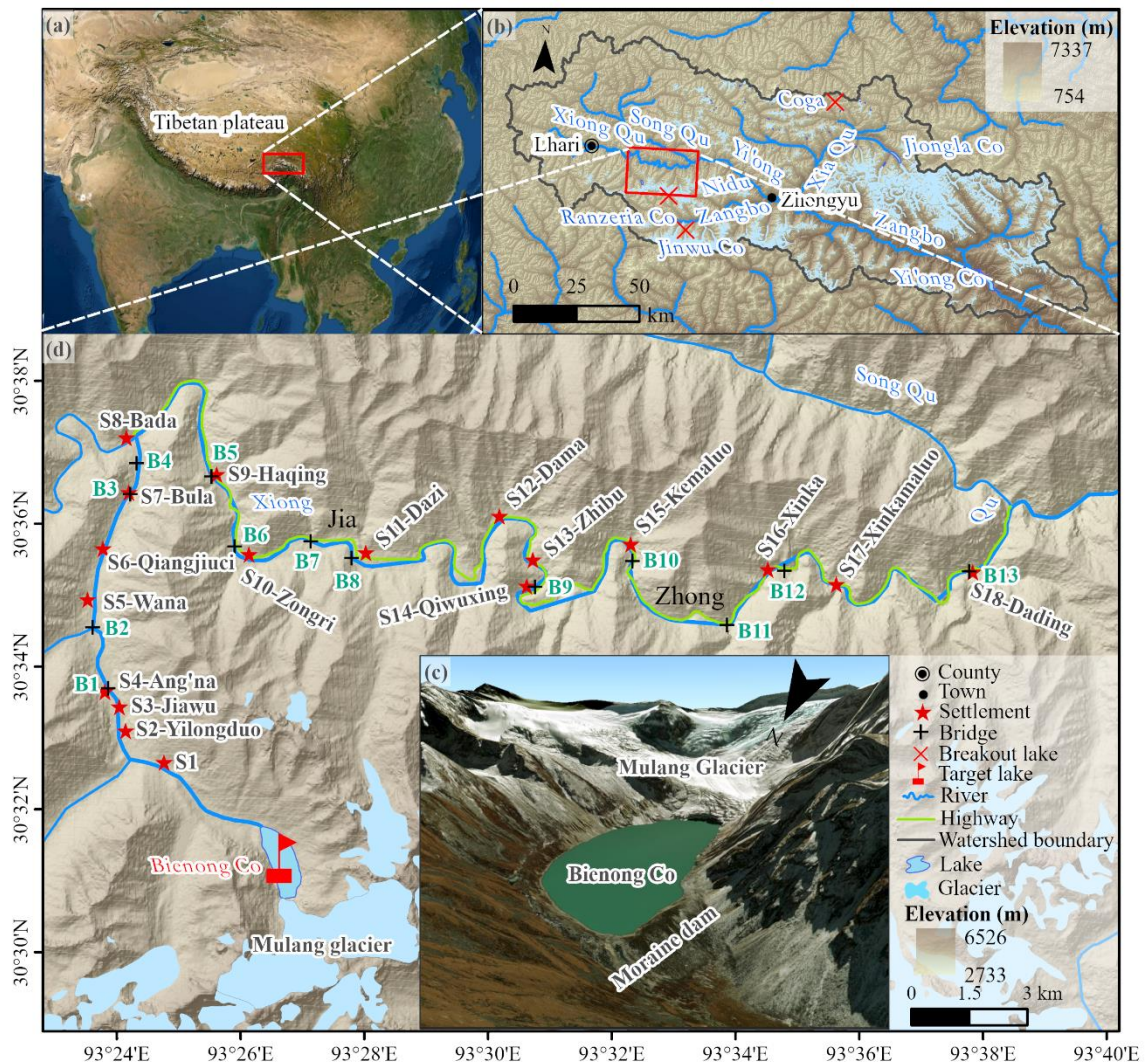


Figure 1. Overview of the study area. (a) The location of the Yi'ong Zangbo basin watershed, (b) the location of Bienong Co, (c) a close view of Bienong Co, and (d) the distribution of settlements, as well as bridges, within ~53 km downstream of Bienong Co. The background of Fig. 1a and c is a MapWorld image, based on which settlements, bridges, and the Jiazhong Highway along the flow channel were identified. The background of Fig. 1b and d is the Advanced Land Observing Satellite's (ALOS) mission Phased Array type L-band Synthetic Aperture Radar (PALSAR) Digital Elevation Model (DEM).

130

The area of Bienong Co has changed minimally over the past 40 years. In 2021, remained basically stable in the past 40 years, but its area of the area of $1.15 \pm 0.05 \text{ km}^2$, in 2021 was almost nearly twice as large as the size of the two nearby outburst moraine-dammed glacial lakes, one of which is Jinwu Co (Zheng et al., 2021) and the other is Ranzeria Co (Sun et al., 2014; Zhang et al., 2022), which were are located just only 24 km and 9 km to the southeast of Bienong Co, respectively. With an average height of 72 m, The moraine dam of Bienong Co's moraine dam has an average height of 72 m, enclosing encloses a water lake volume of $65.2 \times 10^6 \text{ m}^3$, accounting for 64% of the total lake volume (Fig. 2e). Overall, the greater is the volume of water retained in the lake, the greater is the volume of water available for a potential flood ing (Westoby et al., 2014), and the greater is the hazard caused by a GLOFs. GLOFs are highly complex-complicated phenomena, and each one is of which constitutes a distinct, by unique-individual event with characteristics influenced determined by the triggering mechanism, lake hypso metry, geometry geometries, the composition, and structural integrity of the moraine dam, as well as and the

140

topography and geology of the flood-flow path (Westoby et al., 2014). According to historical GLOF studies, the most common cause of glacial lakes' failure in the Himalayas is overtopping and erosion of moraine dams (Risio et al., 2011) triggered by mass movements (snow, ice, or rock, or mixtures) entering lakes (Richardson and Reynolds, 2000; Wang et al., 2012a; Emmer and Cochachin, 2013; Worni et al., 2014), and subsequently overtopping and eroding of the moraine dam (Risio et al., 2011). The Mulang Glacier directly connects Bienong Co; its tongue (here is the ablation zone) contains well-developed ice crevasses with an average slope of 20° (Fig. 2a and b). Bienong Co is directly connected to the Mulang Glacier, whose ablation zone is defined as the mother glacier tongue in this study, and has an average slope of 20° with well-developed ice crevasses (Fig. 2a and b). According to Lv et al., (1999), ice avalanches are more likely to occur when proposed that a slope of the mother glacier tongue slope is greater than 8° - is conducive to the occurrence of ice avalanche. In the context of global warming, glacial Moreover, glacial meltwater can lubricate the glaciers due to climate warming, itself, increasing the likelihood possibility that of overhanging ice will sliding slide into the lakes (Wang et al., 2015). Therefore, ice disintegration from the Mulang Glacier could be a potential trigger for GLOFs of Bienong Co. In a Additionally, the GLOF of Jinwu Co was caused-triggered by an initial moraine landslide with a slope range of 30° - 45° on the left side (Zheng et al., 2021). According to Bolch et al. (2011) and Rounce et al. (2016), both reported that non-glacierized areas around a lakes with a slopes greater than > 30° are potential rock fall, landslide, or other solid mass movement locations regions. Around Bienong Co, multiple places with lateral moraines There are multiple locations with lateral moraines around Bienong Co that fit into this slope range (Fig. 2c, d, and e). Therefore, lateral moraine landslides may could also be a potential trigger offer Bienong Co's GLOF.

The stability of a dam is affected by several parameters, including Dam characteristics, such as dam the geometry (freeboard, width-to-height ratio, distal face slope), dam the material properties, and the ice-cored moraine conditions, govern the stability of the dam (Huggel et al., 2004; Prakash and Nagarajan, 2017 Wang et al., 2011a; Prakash and Nagarajan, 2017 Wang et al., 2011a). Freeboard is refers to the vertical distance between the lake level and the lowest point on the dam crest, which reflects the minimum requisite wave amplitude necessary for overtopping the to occur (Emmer and Vilimek, 2014). rence of overtopping, and a A higher freeboard doesis not favor conducive to the occurrence of overtopping (Emmer and Vilimek, 2014). A natural outlet with a width of ~50 m is in-on the right of the dam (facing downstream) (Fig. 2e and f). As a result, indicating that the freeboard of Bienong Co is 0 m, indicating which signals the a high potential offer overtopping of the lake. The moraine dam has a width of ~520 m and an average height of ~72 m, giving the width-to-height ratio of 7.2 moraine dam is ~520 m wide and the height is variable with an average height of ~72 m, and the width to height ratio is 7.2 (Fig. 2e). According to the thresholds favoring GLOFs of dam widths smaller than 60 m proposed by Lv et al. (1999) and width-to-height ratios smaller than 0.2 proposed by Huggel et al. (2004), the moraine dam of Bienong Co is stable. However, the freeboard of 0 m and the distal facing slope of 35° are conditions that are conducive to GLOFs based on favorable thresholds of smaller than 25 m (Mergili et al., 2011) and larger than 20° (Lv et al., 1999). The surface layer of the moraine dam of Bienong Co is made of larger-grained stones covered with vegetation, the surface layer is a larger particle size of the stone, and be Small granules of loose moraines make up the lower layer the smaller particle size, the material is loose and poorly cemented, which is easily destroyed susceptible to destruction by water forces (Fig. 2e). The existence of ice cores inside within of the moraine dam of Bienong Co is unknown, However, but there is no ice core one in Jinwu Co's breached dam, which is lower ~320 m than the former. The dam crest elevation of Bienong Co is 320 m higher than that of Jinwu Co. Furthermore, Additionally, according to McKillop and Clague (2007), argued that moraine dams with rounded surfaces and minor superimposed ridges are considered ice-cored; in contrast, whereas narrow, sharp-crested moraines with angular cross-sections are interpreted-regarded as ice-free, and † The dam of Bienong Co clearly fits the latter category. In aggregate, we consider that the potential threats to Bienong Co are mainly ice avalanches from the mother glacier and lateral moraine landslides.

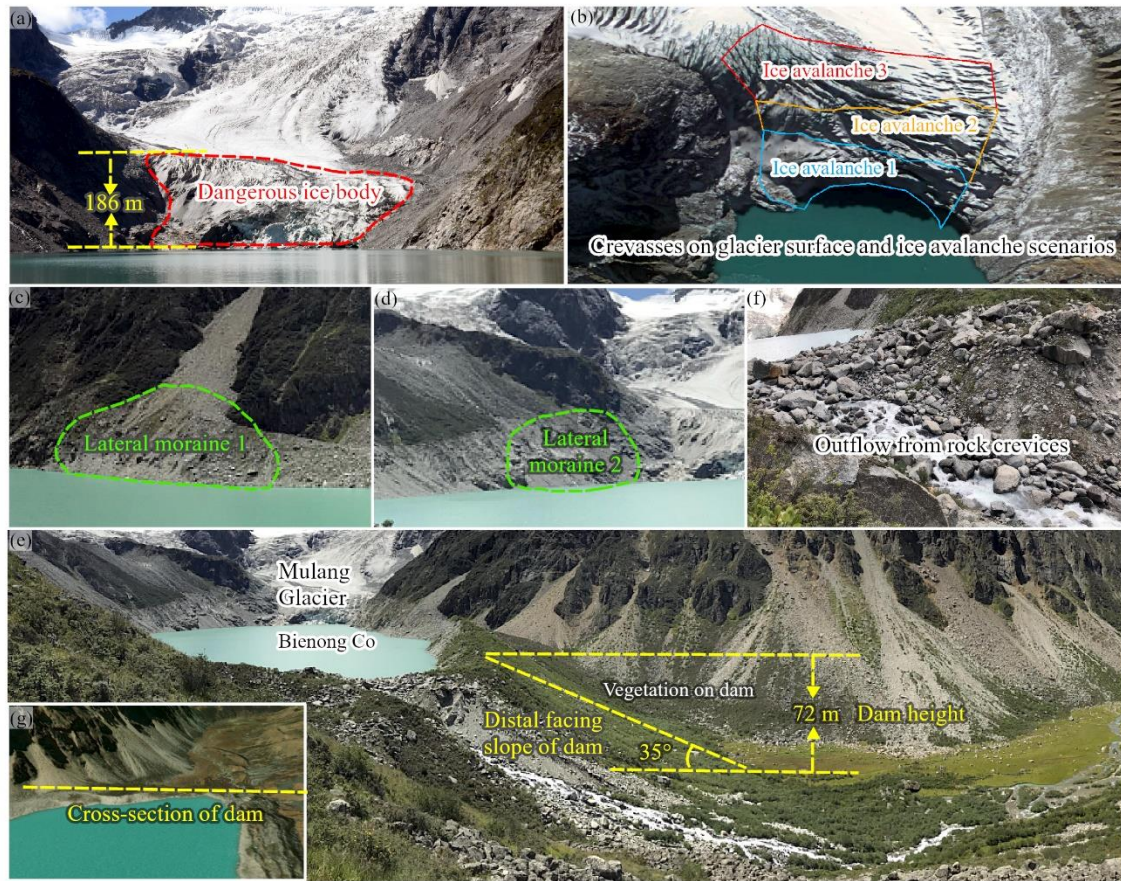


Figure 2. The hazard assessment of Bienong Co. (a) The connection condition of the Mulang Glacier and Bienong Co, (b) the crevasses on the glacier surface and the assumed ice avalanche scenarios of the Mulang Glacier, (c) and (d) the assumed lateral moraine location, (e) and (f) the moraine dam of Bienong Co, and (g) a cross-section of the moraine dam for statistical purposes. Fig. 2(b) and (g) are based on a MapWorld image, and the other photographs were taken by Xiaojun Yao and Qi Wang on August 27, 2020.

3 Methodology

190 3.1 Bathymetry and modeling

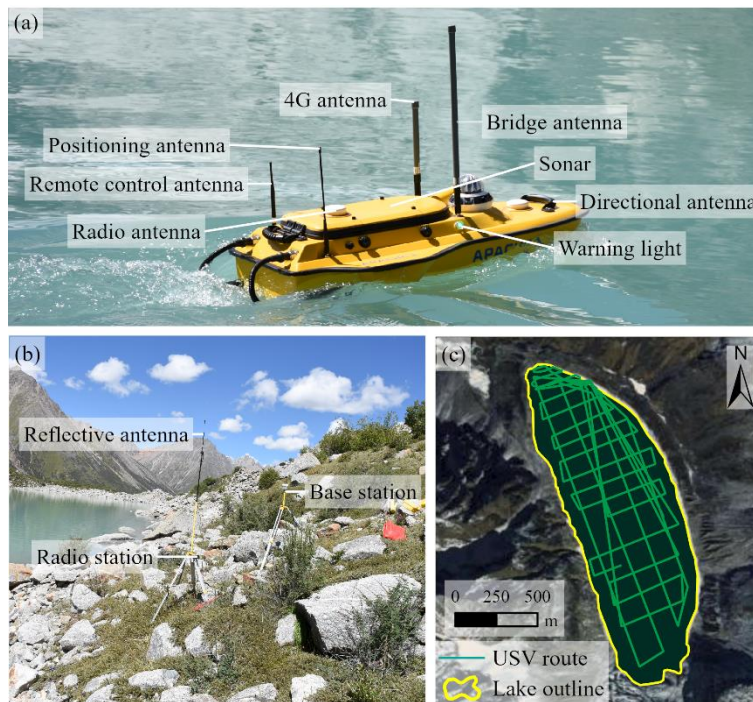
Lake bathymetric ~~information data can be used to depict the underwater topography and calculate the lake volume, which is one of the most important critical inputs parameters for in the dynamic modeling of the GLOFs process chain simulation (Westoby et al., 2014).~~ and can accurately reflect the topography of the lake basin below the water surface and used to calculate the potential flood volume released in different breach scenarios (Westoby et al., 2014). In this study, the bathymetry depth data of Bienong Co were was obtained by a USV (APACHE 3) system, which consists of four main parts: the data acquisition module; the data transmission module; the positioning and navigation control module; and the power module (Li et al., 2021) (Fig. 3a and b). The USV system has a draft of 10 cm, which is smaller than the inflatable kayak used in previous investigations (Haritashya et al., 2018; Sattar et al., 2019, 2021). The D230 Single-Frequency Depth Sounder mounted on the USV ~~has is designed to measure a measurement~~ range of 0.15 - 300 m with a depth resolution of 1 cm and a bathymetry error of $\pm 1 \text{ cm} + 0.1\% \times h$ (water depth). The sounder can operate at 200 kHz and a water temperature range of $-30^\circ\text{C} - 60^\circ\text{C}$. Meanwhile, a real-time kinematic system enables precise positioning for the bathymetric position with a horizontal error of $\pm 8 \text{ mm}$, a vertical error of $\pm 15 \text{ mm}$, and a directional error of 0.2° on the 1 m baseline. Field measurement investigations were as carried out on August 27, 2020. We designed four longitudinal routes and 13 transverse routes ~~prior to before~~ the survey, along which the USV-based measurement was conducted (Fig. 3c). The maximum speed of

205 the USV can reach 8 m/s, and our survey was conducted at a speed of 2 m/s for a total route of 22.58 km in Bienong Co. With no obstructions on the lake, the USV's strong performance and the real-time monitoring allowed the survey to be accurately completed along the designed route. ~~Due to absence of any obstructions on the lake, such as ice or small islands, the high performance of the USV and the real time monitoring, the survey was accurately completed along the designed route.~~ A total of 16,020 valid sounding points were measured, essentially covering the entire glacial lake, ~~were measured~~, which ~~well~~ fulfilled
 210 the data density requirement to model the lake basin topography (Fig.3c).

The DEM of the lake basin~~bathymetric map~~ was created within ArcGIS Pro software using the natural neighbor interpolation algorithm (Thompson et al., 2016; Haritashya et al., 2018; Watson et al., 2018). In addition, Surfer software was employed to simulate the 3D morphology of Bienong Co's lake basin. Lake capacity can be understood as the volume of water storage below a certain water level, which is the volume between a certain spatial curved surface and a certain horizontal
 215 surface (Shi et al., 1991). In this study, the volume of Bienong Co was obtained by multiplying the depth data and ~~map the~~ DEM resolution (5 m) as follows:

$$V = \sum_{i=1}^n H_i \cdot \lambda \quad (1)$$

where V is the volume (m^3) of Bienong Co; H_i is the depth (m) at the i -th pixel; n is the number of pixels in the lake area; and λ is the pixels resolution (m^2) of the DEM of the lake basin~~bathymetric map~~.



220 **Figure 3.** The bathymetry of Bienong Co. (a) The USV sampling equipment in water and (b) on land; (c) the sampling path of USV on Bienong Co covering the base map of the MapWorld image. Photographs were taken by Xiaojun Yao on August 27, 2020.

3.2 Potential GLOF modeling

225 Emmer and Vilímek (2014) and Haeberli et al. (2001) suggested that the assessment of glacial lake hazards should be carried out based on a systematic and scientific analysis of lake types, moraine dam characteristics, outburst mechanisms, downstream processes in the river valley, and possible process cascades. The methodology used in of this study is based on ~~refers to~~ the GLOFs process chain proposed by Worni et al. (2014), which was has been utilized ~~used~~ by Somos-Valenzuela et al. (2016) and Lala et al. (2018) to research study Imja Tsho in Nepal and Palcacocha and Huaraz lakes in Peru, respectively. In this study,
 230 we intend to aim to depict the potential GLOFs triggered~~induced~~ by ice avalanches originating from the mother ~~Mulang~~ g Glacier (Fig. 2a and b) and landslides from the lateral moraine (Fig. 2c and d), ~~and assess potential inundation in the~~

downstream region. The wave resultant from material entering Bienong Co might overtop the moraine dam and initiate an erosive breaching process, releasing considerable amounts of water and debris into the downstream flow channel (Somos-Valenzuela et al., 2016). Three models were used to simulate the GLOFs process chain: the Rapid Mass Movement Simulation (RAMMS) model (RAMMS, 2017) was used to simulate the potential mass movement (Christen et al., 2010); the Basic Simulation Environment for Computation of Environmental Flow and Natural Hazard Simulation (BASEMENT) model (Vetsch et al., 2022) was used to simulate the displacement wave in the lake; and the Heller-Hager model (Heller et al., 2009) was used to calibrate the BASEMENT's results model. The BASEMENT model was also adopted to simulate the dynamic breaching process of the moraine dam, the propagation of the flood wave, and the inundation downstream. In the next following sections, simulation methods for ice avalanches and landslides, displacement waves in lakes, overtopping flow and erosion on the moraine dam, and downstream inundation are described in detail.

3.2.1 Triggers determination and simulation

Ice avalanches are the most common GLOFs trigger in Tibet in China (Yao et al., 2014; Liu et al., 2019). Displacement waves caused by Mass-mass movements into entering a lakes might result in generate impulse waves that may produce overtopping flows that scouring and erosion destroy of the moraine dams, or disrupt the hydrostatic pressure-bearing capacity of the moraine dams. Based on a the investigation survey of the environment surrounding Bienong Co, ice avalanches from the Mulang Glacier and landslides from the lateral moraine landslides at two locations were selected as potential triggers for GLOFs. Wang et al. (2012) defined the dangerous ice volume body of a dangerous glacier as either the volume from the location of the abrupt changing slope to the glacier termini or the volume of the glacier tongue where ice cracks are well developed. We adopted the latter, i.e. In this study, the crevasse-developed ice body of the Mulang Glacier with a surface area of 0.19 km², as shown in the MapWorld image (Fig. 2a) with a surface area of 0.19 km², was selected as the potential ice avalanche source of Bienong Co (Fig. 2a). For convenience of the subsequent description, the ice avalanche-triggered situation was named after Scenario A, we name it Scenario A. The elevation difference between the top of the dangerous ice body and the lake surface was measured to be approximately 155 - 208 m based on ALOS PALSAR DEM. We divided the dangerous ice body into three parts according to elevation ranges as ice avalanche scenarios to simulate subsequent processes from ice avalanches of of different magnitudes (ice avalanche 1, 2, and 3 in Fig. 2b). Scenario A1 was defined as a low-magnitude trigger, and the ice body with an elevation below 4,844 m at an elevation below 4,844 m yields a release area of 0.05 km² with the maximum and average elevation differences of 99 m and 75.8 m from the lake surface, respectively. Scenario A2 was defined as a moderate-magnitude trigger, the ice body at elevation below 4,889 m yields a release area of 0.11 km² with the maximum and average elevation differences of 144 m and 102.7 m from the lake surface, respectively. Scenario A3 was defined as an extreme-magnitude trigger; the total ice body of crevasses with an area of 0.19 km² was set as a release area, with the average elevation difference between the glacier surface and the lake surface of 131 m. In the above three scenarios, we assumed that the release depths of ice avalanches are the average elevation differences from the glacier surface to the lake surface, i.e., the glacier is supported by a flat bedrock located at the height of the lake surface water table.

Lateral moraine landslides as a the GLOFs trigger are not common on the Tibetan Plateau, but the GLOF of Jinwu Co in 2020 was caused by a lateral moraine landslide (Liu et al., 2021; Zheng et al., 2021). Therefore, it, and thus was taken as a trigger of the potential GLOF for Bienong Co. Two areas-locations of lateral moraine within the slope range of 30° - 45° were selected as potential landslide sites, one One of which is located on the left bank (in this study, the left and right sides are defined in a downstream-oriented manner) of Bienong Co, near the moraine dam with an area of 0.015 km², and we named it Scenario B (Fig. 2c). The other Another is located on the right bank, near the mother glacier with an area of 0.024 km², we named it Scenario C (Fig. 2d). Furthermore, we set three different release depths of 2 m (Scenario B1 and C1), 5 m (Scenario B2 and C2), and 10 m (Scenario B3 and C3) for each release area as low-, moderate-, and extreme-magnitude triggers, respectively. Therefore, a total of two different types, three different locations, and nine different magnitudes of materials mass

275 ~~movements entering the lake~~ were designed ~~to enter the lake~~ as ~~the~~ potential triggers ~~for the GLOF of Bienong Co~~ for GLOFs ~~in this study~~. The above design fully considers the impact of triggers on Bienong Co under different magnitudes, and the results are used as the input for the subsequent disaster chain simulation.

In this study, ice avalanches and lateral moraine landslides of Bienong Co were ~~modeled~~ ~~simulated~~ using the Avalanche module of the ~~Rapid Mass Movement Simulation~~ RAMMS model (~~Bartelt et al., 2013~~), which has been successfully used for ~~simulating triggers of GLOFs~~ (Somos-Valenzuela et al., 2016; Lala et al., 2018; Sattar et al., 2021). ~~The~~ RAMMS ~~model~~ adopts 280 the Voellmy-Salm finite volume method to solve depth-averaged equations governing mass flow in two dimensions (Christen et al., 2010). Based on the ~~basic~~ inputs of DEM ~~data~~, the initial release area and depth, the calculation domain, the friction parameters μ (the velocity-independent dry Coulomb ~~term~~) and ζ (~~the~~ velocity-dependent turbulent friction terms), the outputs of runout distances, flow height, and flow velocity can be ~~obtained~~ ~~calculated~~. ~~Then, In addition,~~ the time series of ~~the volume of material mass~~ entering the glacial lake ~~can was taken~~ ~~serve~~ as the input ~~condition~~ for subsequent simulations. For this study 285 case, the initial release area was determined by combining the MapWorld image with a spatial resolution of 0.5 m (<https://www.tianditu.gov.cn/>) and ALOS PALSAR DEM with a spatial resolution of 12.5 m (<https://asf.alaska.edu/datasets/derived-data-sets/alos-palsar-rtc/alos-palsar-radiometric-terrain-correction/>). Values of $\mu=0.12$, $\zeta=1,000 \text{ m s}^{-2}$, and $\rho=1,000 \text{ kg m}^{-3}$ for ice avalanche and $\rho=2,000 \text{ kg m}^{-3}$ for landslide were used, which agree with values used in previous ~~avalanche-induced~~ GLOF ~~studies~~ ~~producing avalanche models~~ (Schneider et al., 2014; Somos-Valenzuela et al., 2016).

290 3.2.2 Hydrodynamic wave simulation

Processes following mass movements ~~s~~ entering the lake, such as the generation and propagation of displacement waves ~~s~~, the overtopping flow and erosion on the moraine dam, and ~~the~~ downstream inundation were modeled using the BASEMENT model ~~v2.8.2~~ (~~Vetsch et al., 2022~~), developed by the Laboratory of Hydraulics, Glaciology and Hydrology (VAW), ETH Zurich. BASEMENT is both a hydrodynamic model and a sediment transport model, making it well suited to model much of the 295 GLOF process chain (Worni et al., 2014). It solves the 2D shallow water equations ~~s~~ (SWEs) in combination with sediment transport equations, primarily the Shields parameters and the Meyer-Peter and Müller (MPM) equations (Vetsch et al., 2022). The simulation of hydrodynamic waves in the lake is performed using the ~~BASEMENT 2D module~~ ~~modeling of BASEMENT~~ based on unstructured grids. The BASEmesh plugin ~~in for~~ QGIS ~~software~~ (QGIS Development Team, 2016) ~~developed by~~ ~~BASEMENT~~ greatly facilitates the generation of mesh. The ~~lake~~ bathymetry data ~~were was produced as a~~ ~~entered into~~ DEM 300 with a spatial resolution of 5 m using ArcGIS Pro software to reflect the ~~topography of Bienong Co's~~ lake basin ~~topography~~. The triangular irregular network (TIN) within the lake ~~area~~ was set to a maximum area of 500 m² to simulate the generation and propagation of ~~hydrodynamic displacement~~ waves in the lake effectively and accurately. The ~~input inflow~~ boundary conditions ~~is are the~~ time series of ice avalanches ~~and or~~ landslides generated by ~~the~~ RAMMS model. ~~In each time period, the~~ ~~The~~ RAMMS ~~model can~~ calculates ~~the sediment volume for each timestep. The time series of ice avalanches or landslides can~~ 305 ~~be determined by counting the sediment volumes within the lake boundary in different timesteps. the total amount of sediment, and the inflow rate can be determined by calculating the difference of sediment entering the lake at two time points. The density of Pure pure~~ rock landslides ~~have been investigated with densities ranging ranges~~ from 1,950 kg m⁻³ to 2,200 kg m⁻³ (Wang et al., 2017), and most ice-dominated avalanches have ~~densities a density~~ of approximately 1000 kg m⁻³. In this study, the ~~densities of ice avalanches and landslides were~~ ~~density was~~ set as 1,000 kg m⁻³; and ~~the landslide density was set as~~ 2,000 kg m⁻³. 310 ~~respectively. Since The~~ BASEMENT ~~model~~ only accepts water as an inflow. ~~Therefore, the densities of ice avalanches and landslides to water are scaled at 1.0 and 2.0 (i.e., 1,000 kg m⁻³ of water is equivalent to 1,000 kg m⁻³ of ice, and only 500 kg m⁻³ of moraine) to accurately describe the momentum transfer of ice avalanches and landslides into the lake.~~ ~~this difference due to density is considered by expanding the landslide material entry rate by a factor of two (i.e., 1,000 kg m⁻³ of water is equivalent to 1,000 kg m⁻³ of ice avalanche volume, and only 500 kg m⁻³ of landslide material), which is the usual~~ 315 ~~approach used in the simulation process~~ (Byers et al., 2018, 2020).

It was shown that the 2D SWEs ~~used by~~ in the BASEMENT model inherently leads to excessive wave attenuation. The Heller-Hager model (~~Heller et al., 2009~~) is a ~~combination~~ ~~combines~~ of analytical and empirical equations ~~used~~ to simulate impulse wave generation, propagation, and run-up ~~resulting~~ from ~~the~~ ~~mass~~ movement ~~of material~~ entering a lake (~~Lala et al., 2018~~). Although the approach relies on simplifying measurements about lake geometry, it has been used to ~~successfully~~ simulate multiple ~~real-actual~~ events ~~successfully~~. ~~and~~ ~~It characterizes~~ ~~performs well in characterizing~~ impulse waves within lakes ~~well~~, making it a simple, but ~~helpful~~ ~~useful~~, calibration measure for more complex hydrodynamic models (Somos-Valenzuela et al., 2016). ~~The~~ BASEMENT ~~model~~ simulated waves ~~are~~ ~~were~~ usually considered more accurate when they ~~are~~ ~~were~~ in ~~of~~ the same order ~~of magnitude as that of magnitude simulated by the~~ ~~as~~ Heller-Hager ~~model~~ ~~waves~~; ~~however~~ ~~However~~, when they ~~are~~ ~~were~~ not, the mass entry rate ~~is~~ ~~was~~ varied by adjusting the inflow hydrograph and boundary width to match the amplitude ~~of the initial wave trajectory near the dam~~ ~~of for~~ the Heller-Hager ~~empirical~~ model ~~near the dam of the initial wave trajectory~~ (Byers et al., 2018; Lala et al., 2018). ~~In this study, we adjusted the wave amplitude near the moraine dam in the BASEMENT model to be close to (difference within 1 m) that calculated by the Heller-Hager model by modifying the width of the inflow boundary.~~ The Heller-Hager model simulates waves in two cases: (a) with longitudinal impacting slide and confined transverse wave propagation; and (b) with the slide impacting across the reservoir and completely free radial wave propagation. In ~~present~~ ~~this~~ study, ice avalanches belong to case (a), and landslides belong to case (b). Compared to case (a), the impulse wave (its amplitude and energy) in case (b) decreases more rapidly because it propagates over a larger area ~~and~~, ~~and~~ is accompanied by wave refraction and reflection.

3.2.3 Moraine dam erosion simulation

~~Overtopping flows are the most common trigger for moraine-dam breaching (Richardson and Reynolds, 2000). The overflow initiates dam erosion, leading to greater outflow and increasing hydrodynamic forces that progressively enlarge the breach (Singh, 1996). Abnormally high lake outflow has the potential to destroy the surface protection layer of the outlet streambed and triggers vertical dam erosion. After the initial cut, more lake water will flow out, followed by an increase in sediment transport rate and a gradual widening of the rift.~~ In this study, hydro-morphodynamic simulations of potential erosion-driven breach failures of Bienong Co were carried out by the BASEMENT model. The model ~~characterizes sediment transports~~ ~~uses~~ ~~using~~ the Meyer-Peter and Müller (MPM) equation ~~to characterize sediment transport~~ and estimates suspended and nudged mass fluxes by calculating the shear stress in the flow through the modified Shields parameter (Vetsch et al., 2022). ~~The overtopping flow leading to erosion of the moraine dam is generated by the wave amplitude of the BASEMENT model calibrated by the Heller Hager model. In the previous step, we adjusted the wave amplitude near the moraine dam in the BASEMENT model to be close to (difference within 1 m) that calculated by the Heller Hager model by modifying the width of the upstream boundary.~~ ALOS PALSAR DEM is the base data for ~~t~~ the mesh ~~generation~~ of the moraine dam ~~with the maximum TIN area of 200 m² was generated from ALOS PALSAR DEM, having a maximum TIN area of 200 m².~~ We set a cross-section along the crest of the moraine dam (Fig. 2g), ~~where at which the erosion of the moraine dam~~ ~~moraine dam deformation, i.e., erosion and, overtopping, as well as outflow discharges,~~ were analyzed. The BASEMENT model provides both single-grain (MPM) and multi-grain (MPM-multi) algorithms to simulate material transport. The MPM-multi ~~algorithm~~ ~~model~~ simulates hiding and armoring processes, ~~potentially leading that may lead~~ to unrealistically low ~~levels of~~ erosion (Vetsch et al., 2022). The MPM ~~algorithm~~ ~~model~~ ignores these processes, however, which can lead to an overestimation of erosion. In this study, we ~~applied~~ ~~used~~ the MPM-multi ~~algorithm~~ ~~model~~ to simulate bed-load transport of the moraine dam, ~~which is~~ composed of materials ~~of with~~ different grain sizes. ~~In addition, a correction factor of 2.0 was used to increase the bed load transport rate. Values between 0.5 (low transport) and 1.7 (high transport) are generally realistic (Wong and Parker, 2006); whereas a value of 2.0 provides high sediment transport conditions (Somos-Valenzuela et al., 2016) to compensate for the lower erosion of the MPM-multi algorithm.~~ The specific grain size distribution ~~of Bienong Co's moraine dam~~ was not measured; ~~but~~ ~~It~~ was instead taken from an inventory of glacial lakes in the Indian Himalayas (Worni et al., 2013) that had

performed well in recreating previous GLOFs in Nepal (Byers et al., 2020). ~~Despite uncertainty in the actual grain size distribution, a similar GLOF modeling study in the Barun Valley (Byers et al., 2018) found little difference in simulated moraine erosion between the grain size distributions listed in Worni et al. (2013).~~ The moraine dam of Bienong Co consists of ~~a large grains cover~~ with a thickness of approximately 0.5 m at the top and ~~fine-small grains~~ underneath, which is clearly visible on the side walls of the channel scoured by water (Fig. 2e). We set two soil layers in the BASEMENT model to represent the above situation. The ~~upper layer with the large largest particle grain size~~ ($d_{50} = 180$ mm) ~~in the upper layer with~~ has a depth of 0.5 m; ~~and the lower layer with the grain size distribution same as Worni et al. (2013) of the lower layer with~~ has a depth of 71.5 m (considering the mean height of moraine dam of 72 m). ~~are consistent with Worni et al. (2013). Finally, a correction factor of 2.0 was used in the model to increase the rate of bed load transport. Values between 0.5 (low transport) and 1.7 (high transport) are generally realistic (Wong and Parker, 2006); whereas a value of 2.0 provides high sediment transport conditions (Somos Valenzuela et al., 2016) to compensate for the lower erosion of the MPM multi model.~~

3.2.4 Downstream impact analysis

The flow channel from Bienong Co to the convergence with Song Qu stretches ~53 km (Fig. 1d), along which 18 settlements, 13 bridges, and the Jiazhong Highway are distributed. ~~In this study used, the BASEMENT model was used to simulate the hydrodynamic behavior of potential GLOFs along the flow channel, and We assessed the hazard of floods-GLOFs was assessed by analyzing the inundation areextent and depth, flow velocity, and flood arrival time at these settlements. The BASEMENT 2D module model for an unsteady hydraulic simulation requires inputs of terrain data and boundary conditions.~~ The terrain ~~data were~~ was represented by a 2D mesh covering the entire flow ~~areachannel, which was~~ obtained from ALOS PALSAR DEM. The mesh was also generated by the BASEmesh plugin of QGIS software, and the ~~maximum TIN individual cell areas for of~~ the main flow channel and other regions were set ~~to as~~ 500 m² and 5,000 m², respectively, ~~considering for~~ the accuracy requirements of the simulation and the computational efficiency of the model. ~~The friction of the a river flow channel to a given flow was determined by the Manning's roughness coefficient (Coon, 1998), which is dependent on the land use and land cover of the modeling river channel in the study area.~~ In this study, the GLC10 LULC product (http://data.ess.tsinghua.edu.cn/fromglc10_2017v01.html) with a spatial resolution of 10 m was used to obtain the value of Manning's N in the flow channel. The ~~upstream-inflow~~ boundary is the outflow hydrograph from the ~~lake moraine dam simulated by the BASEMENT model.~~ The ~~downstream-outflow~~ boundary is the water level-discharge relationship of the cross-section ~~in the downstream, boundary of the simulation area, and was~~ estimated by the critical depth method (Byers et al., 2018).

385 4 Results

4.1 Morphology and lake volume estimation of Bienong Co

The basin morphology of Bienong Co was modeled based on ~~the TIN grid created by the field bathymetry depth~~ data (Fig. 3). ~~As shown in Fig. 4, Apparently, this lake has a relatively flat basin bottom, and steep both flanks are deep (Fig. 4). The slope of the lake shore near the glacier is steeper than that near the moraine dam, which is Similar-similar to most moraine-dammed~~ glacial lakes (Yao et al., 2012; Zhou et al., 2020), ~~the slope of the lake shores near the glacier is steeper than that near the moraine dam.~~ The water depth profile from the moraine dam to the mother glacier shows that the ~~lake's~~ depth ~~of the lake~~ reaches a maximum of ~181 m at approximately 1,000 m from the moraine dam, corresponding to a slope of 11.3°. The depth remains stable ~~at the distance of~~ 1,000 m to 1,500 m from the moraine dam; ~~and~~ ~~The distance from the Mulang Glacier to the deepest point of the lake is 600 m with a slope of 16.5°. A depth profile facing the moraine dam from the left bank to the right~~ bank shows that the left side is steeper than the right side. The glacial lake reaches its deepest point at 200 m from the left shore with a slope of 43.4°, then remains flat to 430 m, and the distance between the bottom and ~~the~~ right shore is 273 m with

a slope of 32°. The volume of Bienong Co, calculated using the surface elevation and the lake bed derived from the TIN grid, was approximately $102.3 \times 10^6 \text{ m}^3$ in 2020, which is a generally accurate estimate of the magnitude of this moraine dammed lake.

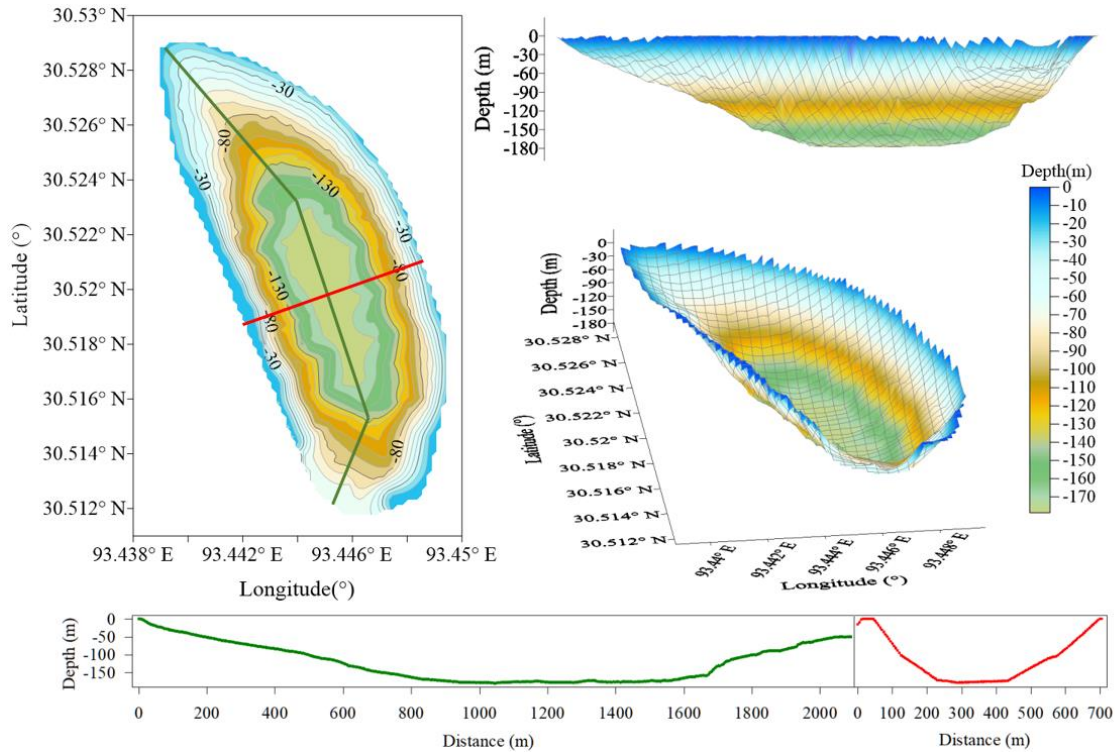


Figure 4. Morphology modeling of Bienong Co in 2020, and equal-scale profiles of distance and depth from the moraine dam to the Mulang Glacier (green line) and from the left shore to right shore (red line).

4.2 Potential GLOFs modeling

4.2.1 Ice avalanches and lateral moraine landslides

As calculated by RAMMS, the volumes of ice avalanches entering Bienong Co for Scenarios A1, A2, and A3 are $3.8 \times 10^6 \text{ m}^3$, $4.9 \times 10^6 \text{ m}^3$, and $5.8 \times 10^6 \text{ m}^3$ (Fig. 5a), respectively. Most of the materials-ice body enter the lake within approximately 120 s. Based on the area of $\sim 1.15 \text{ km}^2$ in 2021, the above three scenarios could result in a rise of approximately 3.3 m, 4.2 m, and 5.1 m in the lake surface, respectively. Material-The volumes of landslides entering the lake by both landslides are much smaller than those of the ice avalanches (Fig. 5b and c). In Scenarios B1, B2, and B3 and C1, C2, and C3, dump the volumes of moraines entering the lake are $0.03 \times 10^6 \text{ m}^3$, $0.09 \times 10^6 \text{ m}^3$, and $0.17 \times 10^6 \text{ m}^3$, and $0.06 \times 10^6 \text{ m}^3$, $0.15 \times 10^6 \text{ m}^3$, and $0.30 \times 10^6 \text{ m}^3$ of mass volume into the lake, respectively. It takes less time for the moraines to enter the lake, The time for materials entering the lake is less than in Scenario A, with Scenarios B1-3 being completed in approximately 10 s and Scenarios C1-3 in approximately 15 s.

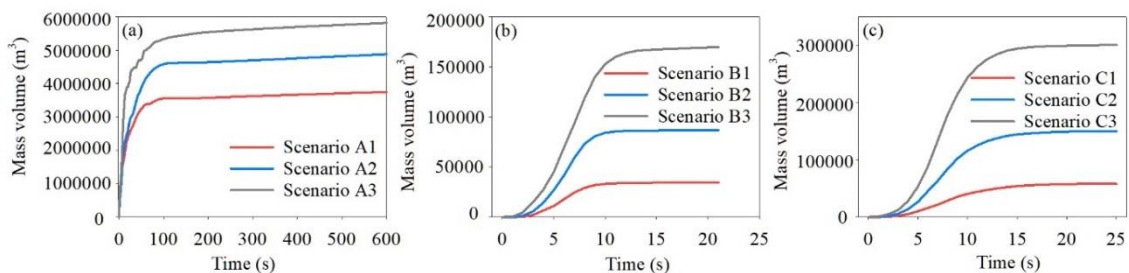


Figure 5. Volume of material entering Bienong Co for different (a) ice avalanche scenarios and (b) and (c) landslide scenarios.

The impact area-zones caused by material-mass entering the lake differs for different scenarios. They are 0.27 km², 0.31 km², and 0.38 km² impact-zones caused by-for Scenarios A1, A2, and A3 are 0.27 km², 0.31 km², and 0.38 km², with horizontal distances of 549 m, 629 m, and 752 m from the upper-inflow boundary, respectively (Fig. 6). In contrast, each of these three scenarios for Scenarios B and C result in a-the relatively small impact zones, with Scenario C3 being the largest at-of 0.14 km² and Scenario B1 being the smallest at-of 0.04 km². Scenarios A1, A2, and A3 produce the maximum flow heights of 39.5 m, 46.2 m, and 53.5 m, and the average flow heights of 12.2 m, 14.6 m, and 12.3 m in the impact area-zones, respectively. The maximum and the average flow heights of Scenarios B1, B2, and B3 range from-Scenarios B1, B2, and B3 is 6.8 m to- 14.6 m and, and the average flow height range is- from 1.8 m to- 3.5 m, respectively. The ranges of the maximum and average flow heights ranges for-of Scenarios C1, C2, and C3 are 5.7 - 29.2 m and 2.0 - 4.7 m, respectively (Fig. 6). The maximum flow velocities for-of Scenarios A1, A2, and A3 are 34.9 m/s, 43.1 m/s, and 51.4 m/s, with average flow velocities of 11.1 m/s, 12.3 m/s, and 16.8 m/s, respectively. The maximum and average flow velocities offer Scenarios B1, B2, and B3 and C1, C2, and C3 are in the range of 21.3 - 33.6 m/s and 8.5 - 14.2 m/s, respectively (Fig. 6).

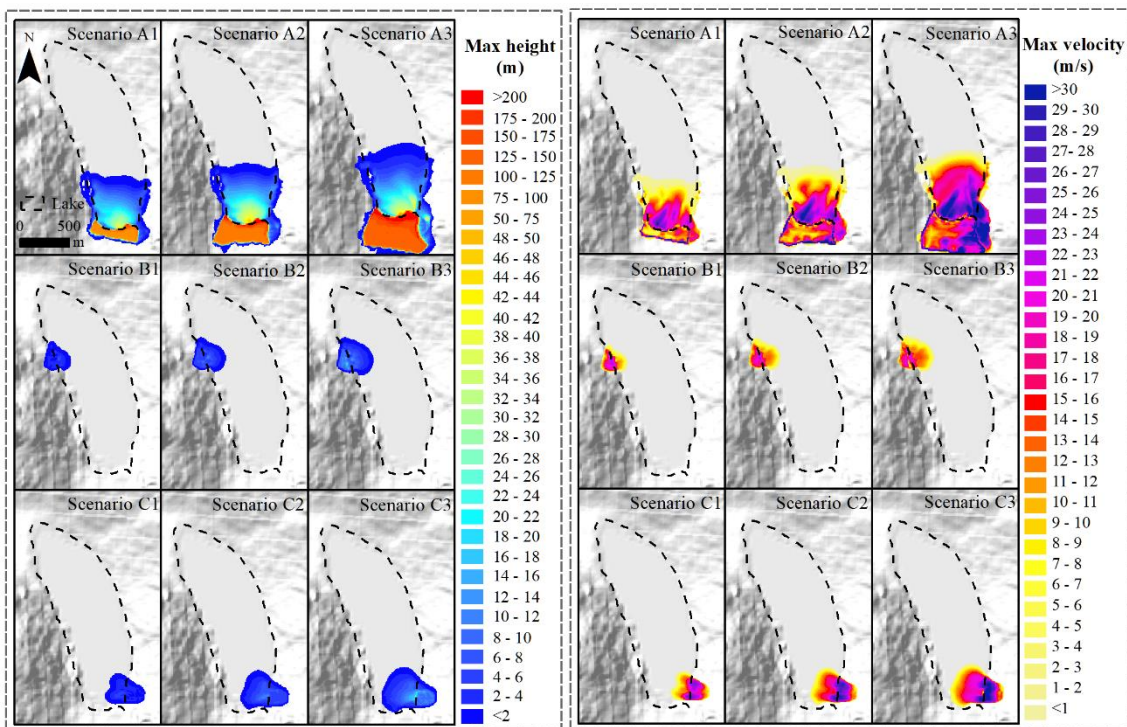


Figure 6. Maximum flow height (left) and maximum flow velocity (right) for different ice avalanches and landslides scenarios.

4.2.2 Generation and propagation of displacement waves

By counting material-the mass volumes of ice avalanches and landslides entering Bienong Co in-at different time steps periods based on the RAMMS model, we derived the time series of the material-mass-entering rate, as shown in Fig. 7. Compared to Scenarios A2 and A3, Scenario A1 has the highest peak flow rate of 439,952.57 m³/s, but however, it decreases rapidly after reaching the peak within 2 s of the ice avalanche, i.e., the ice avalanche occurs in a moment. Scenarios A2 and A3 exhibit apparent-obvious fluctuations in the process of ice avalanches into-entering the lake, with sub-peaks in-both scenarios that are comparable to the first-peaks, after which the flow rates still possess strong fluctuations. The peak and sub-peak flow rates of Scenarios A2 and A3 are 263,922 m³/s and 238,086 m³/s as well as 386,359 m³/s and 373,449 m³/s, respectively, both occurring at the 2nd and 8th seconds of the ice avalanches. Scenarios A2 and A3 have the larger volumes of ice avalanches and the further transfer distances than Scenario A1, leading to a more complex process of ice bodies entering the lake. This is because the ice avalanches of Scenarios A2 and A3 are further away from the lake than Scenario A1, and total volumes of ice avalanches are larger than Scenario A1, and thus they undergo a more complex process when they enter the lake. The process of landslide moraines entering the lake is simpler in Scenarios B and C. The peak flows increase sequentially from Scenarios B1 and C1,

445 B2 and C2, to B3 and C3, with peak values of Scenarios B3 and C3 of 50,849 m³/s and 92,529 m³/s for Scenarios B3 and C3, respectively, which are the peak flow for Scenario B3 is approximately 3.8 times and 6.5 times that of Scenarios B1 and C1, respectively. The peak flows for the six scenarios of Scenarios B and C occur in the range of 6 - 8 seconds (Fig. 7).

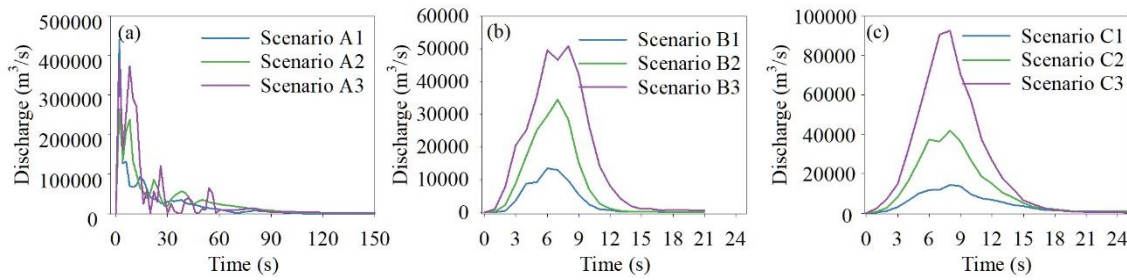


Figure 7. Time series of material entry into the lake for different ice avalanche and landslide scenarios.

450 The time-volume relationships of materials mass entering a lake have has an important effects on the generation and propagation of displacement waves in the a lake. Ice avalanche scenarios (A1, A2, and A3) have a much greater impact on Bienong Co than the two landslide scenarios (B1, B2, B3, C1, C2, and C3) because the assumed release volumes of ice avalanches is are much greater than that of landslides. The wave height near the moraine dam is the result of the BASEMENT model calibrated by the Heller Hager model. By adjusting the inflow boundary's width, we made the BASEMENT model produce wave amplitudes near the dam with a difference smaller than 1 m of those calculated by the Heller Hager model, which is important for subsequent simulations, although the maximum wave amplitude in the lake is exaggerated. In Scenario A, displacement waves propagate straight from the glacier to the moraine dam, and arrive arriving at the vicinity of the moraine dam at approximately 70 s. Scenarios A1, A2, and A3 produce the highest wave amplitudes in the lake of 35.2 m, 39.0 m, and 66.4 m, respectively, and the wave amplitudes near the moraine dam of are 17.1 m (72 s), 20.2 m (74 s), and 25.2 m (72 s), respectively (Fig. 8). Compared with Scenario A, the wave amplitudes of Scenarios B and C are markedly lower. In Scenario B, a the landslides occurs at the left shore of Bienong Co near the moraine dam (Fig. 2c). The Displacement displacement waves first propagate to the opposite shore in a perpendicular direction to the inflow boundary, and then they propagate to the moraine dam with the expansion. The maximum wave amplitudes in Bienong Co of Scenarios B1, B2, and B3 are 6.5 m, 14.1 m, and 18.0 m, respectively, and the wave amplitudes near the moraine dam are 1.2 m, 3.0 m, and 5.3 m, respectively (Fig. 8). The landslides in Scenario C occurs on at the right bank shore of Bienong Co near the Mulang glacier Glacier. The displacement waves propagate in a the same manner way as that in Scenario B, in which waves propagate to the opposite bank shore first after moraines aterials enter the lake, with the maximum wave amplitudes of 4.8 m, 9.6 m, and 24.7 m for Scenarios C1, C2, and C3, respectively. Unlike Scenario B, displacement waves in Scenario C cross the entire lake, reaching the moraine dam with wave amplitudes of 0.6 m, 2.2 m, and 4.9 m near the moraine dam, respectively (Fig. 8). Therefore, although the volumes of landslides volume of in Scenario C is are larger than that those in of Scenario B, the wave amplitudes near the moraine dam are smaller than those of in Scenario B.

465

470

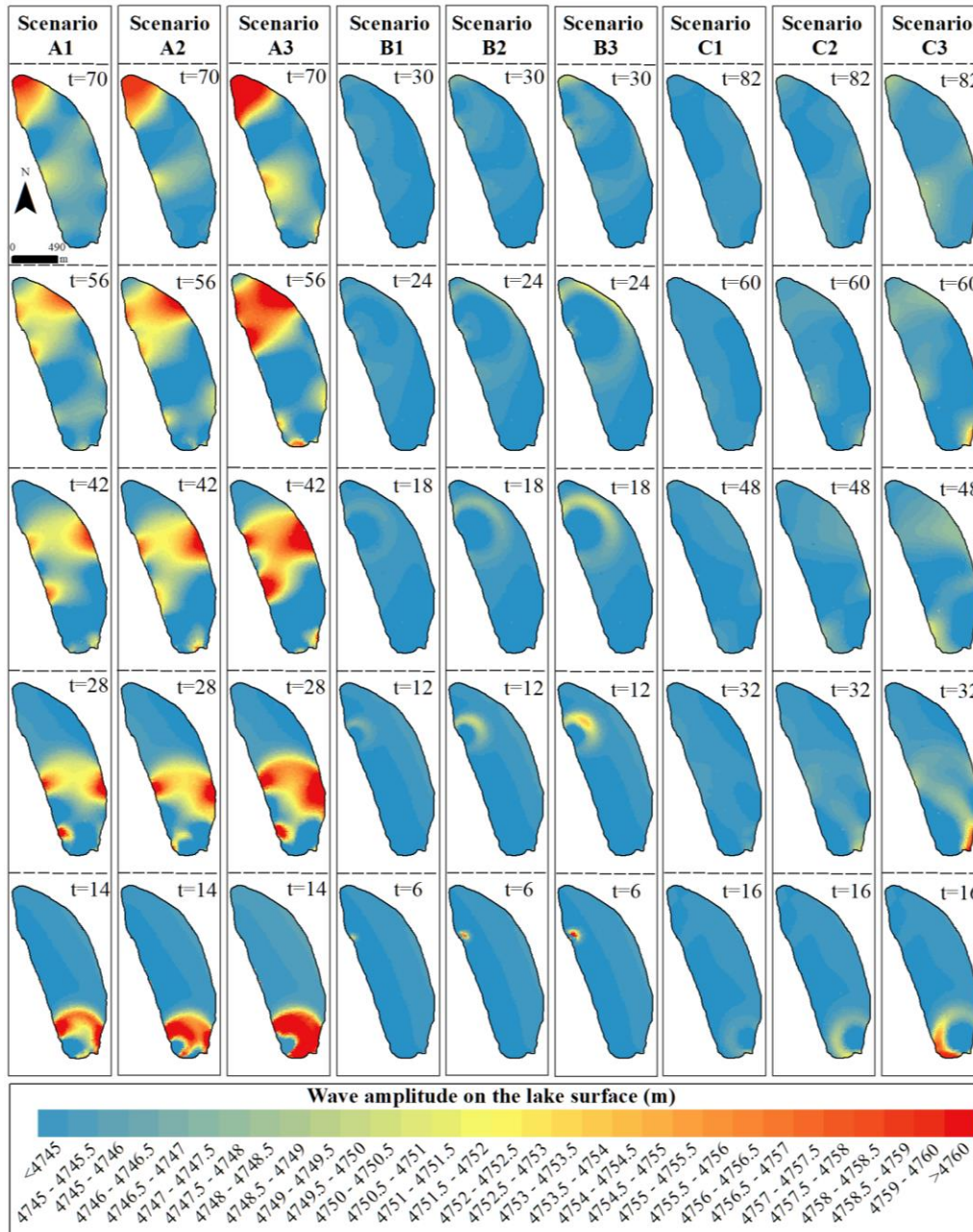
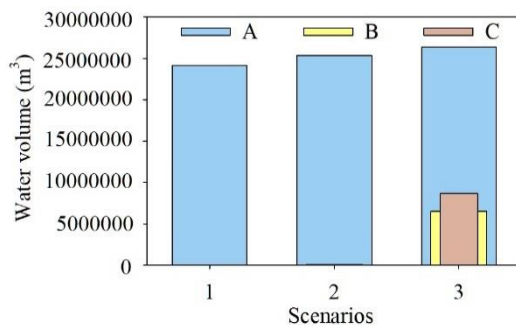


Figure 8. Propagation of displacement waves in the lake for different ice avalanches and landslide scenarios.

4.2.3 Overtopping flow and erosion on the moraine dam

Since the freeboard of the moraine dam is 0 m, the occurrence of overtopping flow is inevitable in all scenarios, but there are differences in magnitude. In Scenarios A1, A2, and A3, the moraine dam is eroded by enormous discharges, forming a breach. The peak discharges at the breaches of the moraine dam are $4,996 \text{ m}^3/\text{s}$, $7,817 \text{ m}^3/\text{s}$, and $13,078 \text{ m}^3/\text{s}$, corresponding to a total released volume of $24.1 \times 10^6 \text{ m}^3$, $25.3 \times 10^6 \text{ m}^3$, and $26.4 \times 10^6 \text{ m}^3$, respectively (Fig. 9). The Discharges discharges at the moraine dam stabilize after ice avalanches enter Bienong Co at approximately 18,000 s, 10,800 s, and 7,200 s, respectively. Therefore, the erosion of the moraine dam and the total volume of water lost in from the lake were counted based on the above time points. The moraine dam is eroded by enormous discharge output in Scenarios A1, A2, and A3, forming breaches. Due to the similar volume of water released water in Scenarios A1-3, the depth of the breach is are similar, slightly different for Scenarios A1, A2, and A3, which are approximately 19.0 m, 19.1 m, and 19.3 m, respectively (Fig. 10). Moreover However, the peak discharges is quite different for the three scenarios, resulting in different breach widths of 295.0 m, 339.4 m, and 368.5 m, respectively. Scenarios B1, B2, and B3 and C1, C2, and C3 resulted in overtopping flows of $0.6 \times 10^6 \text{ m}^3$, $1 \times 10^6 \text{ m}^3$, and 2.6

485 $\times 10^6 \text{ m}^3$, and $0.1 \times 10^6 \text{ m}^3$, $0.9 \times 10^6 \text{ m}^3$, and $3.4 \times 10^6 \text{ m}^3$, respectively, in which only Scenarios B3 and C3 cause erosion of the moraine dam and form a breach. **In Scenarios B3 and C3, the discharges at the breach become stable beginning after 18,000 s following of landslide moraine material entry into the lake in Scenarios B3 and C3. The peak discharges are $504 \text{ m}^3/\text{s}$ and $733 \text{ m}^3/\text{s}$, with breach depths of 6.5 m and 7.9 m, and breach widths are of 153 m and 169 m with peak discharges of $504 \text{ m}^3/\text{s}$ and $733 \text{ m}^3/\text{s}$, respectively.**



490 **Figure 9.** Discharge of water bodies in glacial lakes under different scenarios.

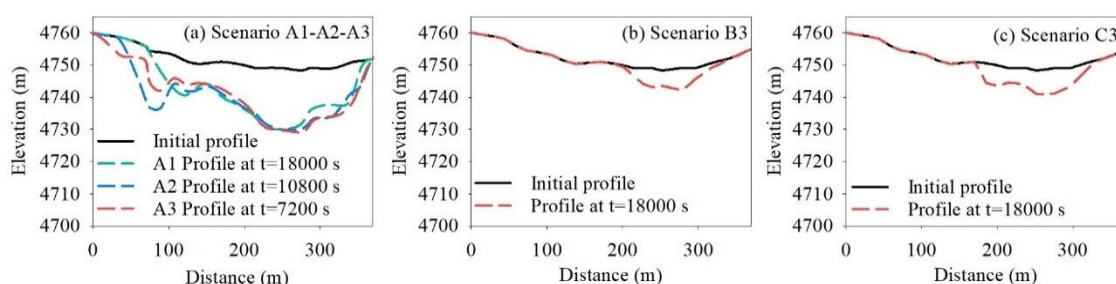


Figure 10. Erosion of the moraine dam under different conditions at the cross-section in Fig. 2g.

4.2.4 GLOFs impact in the downstream region

495 The hydraulic behavior of GLOFs in the flow channel ~~from immediately downstream of the~~ moraine dam to the convergence with Song Qu ~~with the distance of (~53 km)~~ was simulated using the BASEMENT model. ~~The small baseflows in the flow channel were neglected. Due due~~ to the lack of reliable data, ~~on small baseflows in the flow channel, they were neglected in the simulation.~~ Considering the ~~differences between~~ propagation of floods in different scenarios, we ~~evaluated assessed~~ the propagation of GLOFs in the downstream channel within 20 h ~~from ice avalanche and landslide materials entry into the lake.~~

500 ~~The Peak-peak~~ discharges ~~at the breach of Scenarios A1, A2, and A3 at the breach~~ are $4,996 \text{ m}^3/\text{s}$, $7,817 \text{ m}^3/\text{s}$, and $13,078 \text{ m}^3/\text{s}$, respectively, ~~outlet of Scenarios A1, A2, and A3~~ all occurring approximately 600 s after ~~the ice bodies avalanche material enters~~ the lake, ~~and they are $4,996 \text{ m}^3/\text{s}$, $7,817 \text{ m}^3/\text{s}$, and $13,078 \text{ m}^3/\text{s}$, respectively, based on which GLOFs of the three scenarios~~ floods all pass through 18 settlements in the downstream river flow channel in 20 h. ~~with the~~ The inundation areas of Scenarios A1, A2, and A3 are 7.6 km^2 , 8.0 km^2 , and 8.5 km^2 , respectively, with as well as the average water depths of 8.4 m, 9.1 m, and

505 10.0 m, respectively (Fig. 11). Scenarios B1 and C1 ~~only~~ result in small overtopping flows, with peak discharges of $106 \text{ m}^3/\text{s}$ (after 40 s) and $12 \text{ m}^3/\text{s}$ (after 50 s), respectively. ~~have a small volume of overtopping flow from the lake (peak discharges of $106 \text{ m}^3/\text{s}$ (after 40 s) and $12 \text{ m}^3/\text{s}$ (after 50 s)), and fail to generate runoff downstream of the dam.~~ Scenarios B2 and C2 produce very limited overtopping flows with peak discharges of $177 \text{ m}^3/\text{s}$ (after 240 s) and $186 \text{ m}^3/\text{s}$ (after 480 s), respectively, and outflows remain only within approximately 1 km downstream of the moraine dam. Peak discharges at the breach-outlet of

510 Scenarios B3 and C3 are $504 \text{ m}^3/\text{s}$ (after 240 s) and $733 \text{ m}^3/\text{s}$ (after 480 s), yielding inundation areas of 1.7 km^2 and 2.2 km^2 with average water depths of 1.9 m and 2.4 m in the downstream region, respectively. Both GLOFs pass through the first eight settlements, but the flood of Scenario C3 flows farther (Fig. 11). ~~Among In~~ the nine scenarios ~~that we considered~~, only Scenarios A1, A2, A3, B3, and C3 result in ~~caused~~ GLOFs ~~propagation propagating~~ in the downstream region ~~flow channel~~ ~~over~~ with a far considerable distance, ~~in which~~ Scenario A3 ~~had has~~ the largest largest flood magnitude, ~~whereas and~~ Scenario

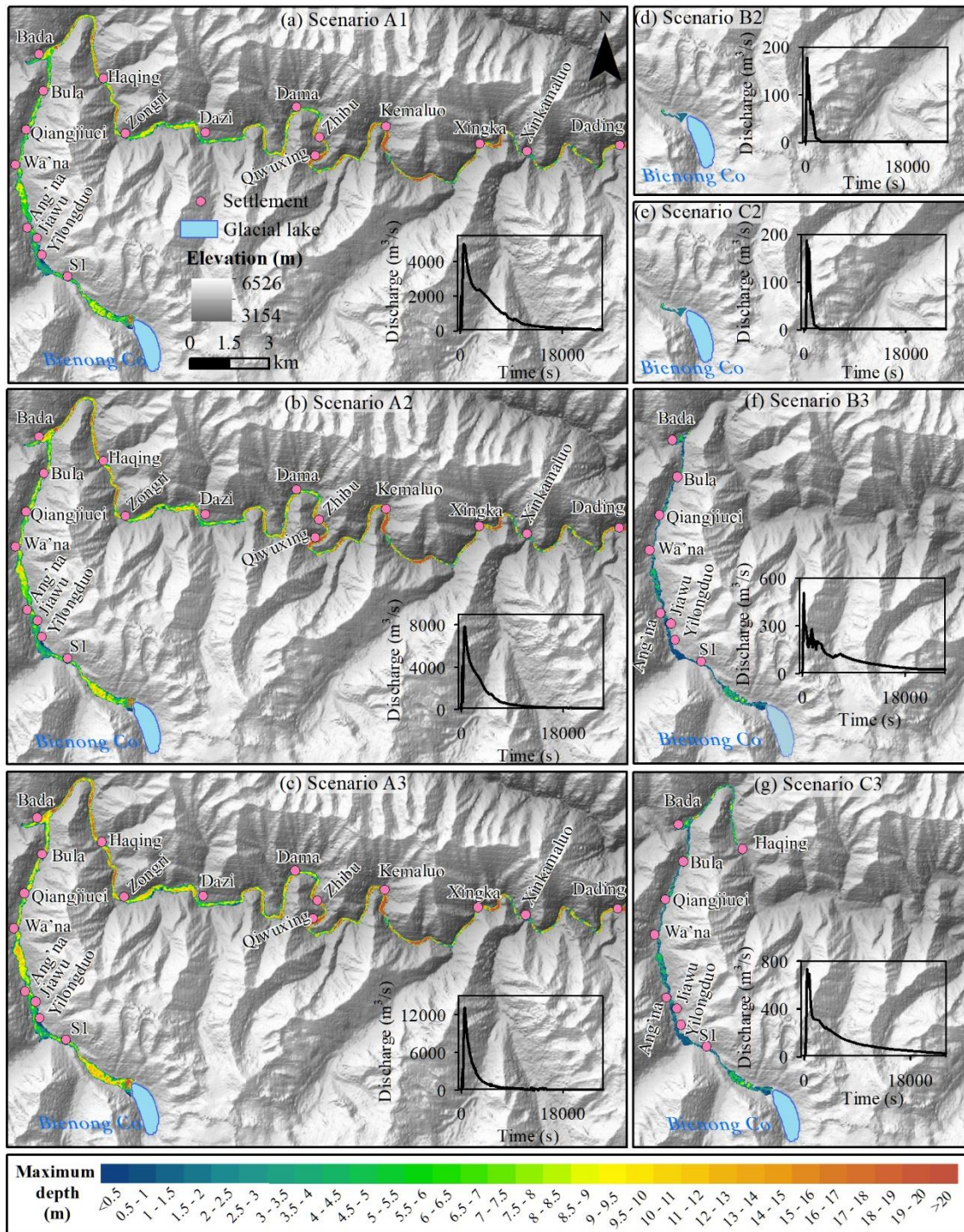
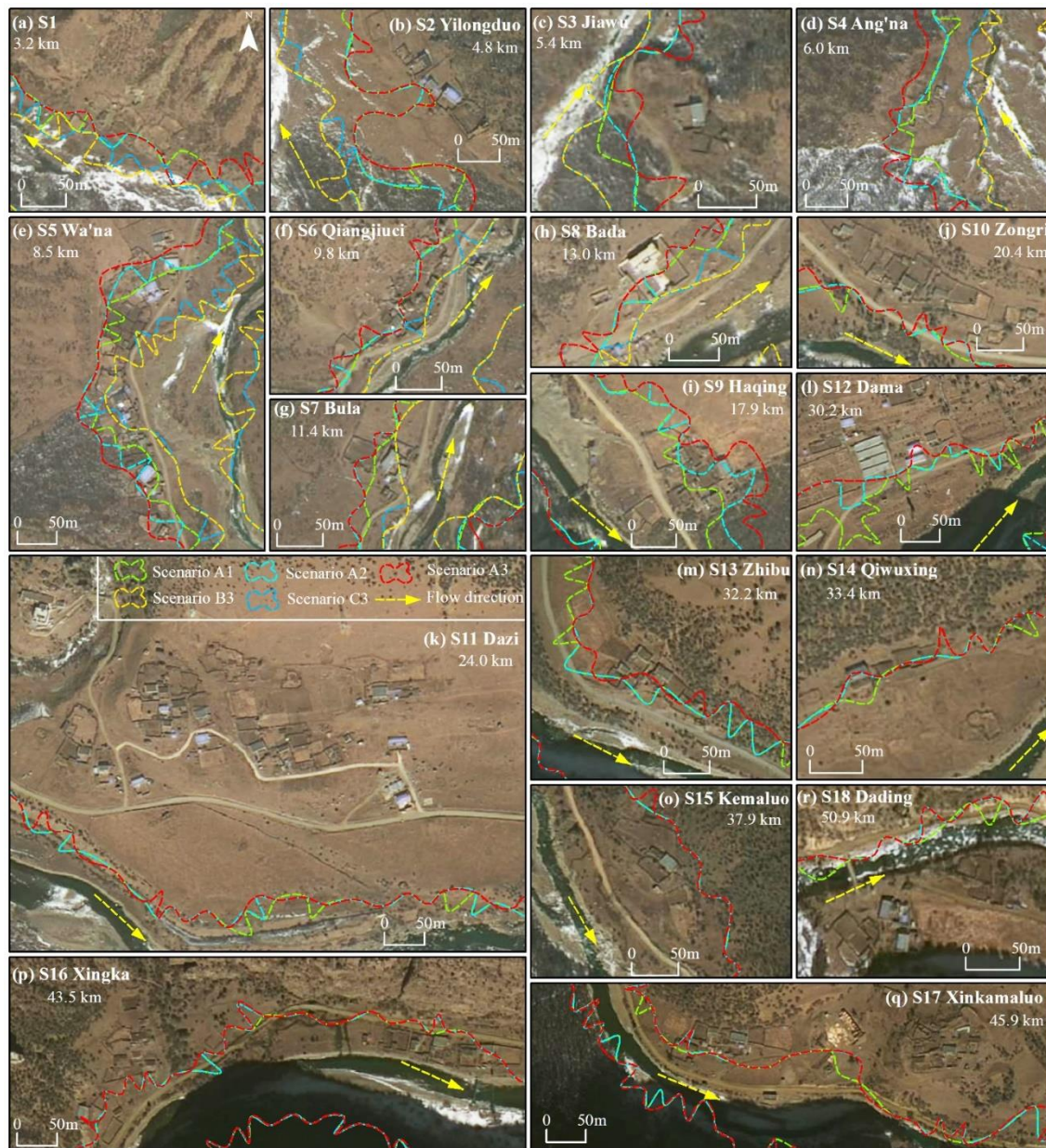


Figure 11. Propagation of flood water downstream and the time series of discharge at the breach outlet (inset) for different scenarios.

GLOFs of different magnitudes pose different potential hazards to each settlements along the flow channel. Scenario A3 produces the most severe threat of GLOF to the downstream region. Six settlements are entirely submerged by flooding, including Ang'na, Wa'na, Haqing, Kemaluo, Xinka, and Dading, will be completely submerged by flooding. Kemaluo village, located 37.9 km downstream of Bienong Co, will experiences the relatively-largest maximum flow depth of 19.8 m, and the village of Ang'na, having a distance of 6.0 km from Bienong Co, will experiences the relatively-smallest maximum flow depth of 6.1 m. Wa'na is the village is the-most affected of all of the villages by GLOFs due to the largest flooded area, most flooded houses. Eight settlements are partially flooded, including S1, Qiangjiuci, Bula, Bada, Dama, Zhibu, Qiwuxing, Xingka, and Xinkamaluo. The maximum flow depth in Bada village is the largest (11.0 m). The maximum flow

depth of 11.0 m; in Bada village is the largest, and that in Dama village and Zhibu village is the smallest (7.2 m) that of 7.2 m in both Dama and Zhibu villages is the smallest. Four settlements, Yilongduo, Jiawu, Zongri, and Dazi, are spared from floods; in Among them, which Yilongduo village may be slightly affected; while Dazi is the safest village due to its far distance from the river. Flooding The GLOF in of Scenario A2 has a relatively small minor impact on downstream villages compared to that of than that of Scenario A3, with showing the reduced extent of inundation extent and flow depth. The flooding extents in Ang'na and Haqing villages have a reduction have been reduced. However, The villages of Wa'na, Kemaluo, Xinka, and Dading are will still be completely entirely flooded, however, but the maximum flow depths is are decreased reduced from 16.5 m, 19.8 m, 12.5 m, and 17.5 m, to 13.6 m, 19.3 m, 12.0 m, and 16.6 m, respectively. For The nine villages that are partially affected in by Scenario A2 A3, they are still affected by flooding of Scenario A2 except for Dama village, but the impact magnitude of flooding is diminished. Scenario A1 differs from Scenario A3 in that the villages of Dama and Xingkamaluo villages were are spared from the flooding, while and other villages experienced significant greatly reduced tions in flooding extent and inundation depth. The GLOFs of Scenarios B3 and C3 have a significantly minor impact in on the downstream flow channel than Scenarios A1, A2, and A3. Only Wa'na Wa'na, Qiangjiuci, and Bula villages will bear partially affected, with the maximum flow depths of 3.1 m, 1.9 m, and 2.0 m in Scenario B3 and 4.0 m, 2.4 m, and 2.7 m in Scenario C3, respectively (Fig. 12). The total areas of houses, courtyards, and farmlands (around settlement) affected by Scenarios A1, A2, A3, B3, and C3 were are estimated to be 23,984 m², 32,076 m², 41,038 m², 3,820 m², and 3,918 m², respectively. In Scenarios A1, A2, and A3, all 13 bridges and approximately 35 km of roads (including the Jiazhong Highway) with a length of approximately 35 km are within the flood zones, and in Scenarios B3 and C3, there are four bridges as well as and approximately 3.6 km and 6.7 km of roads with a length of approximately 3.6 km and 6.7 km with are in the flood zones. Here we only assess the potential impact of floods GLOFs on these man-made artificial structures, but the concrete impact magnitude of the impact is beyond the scope of this study.

The p Peak discharges and velocity velocities of GLOFs gradually decrease in these villages from upstream to downstream, experience a gradually decreasing process; Meanwhile, while the arrival times of peak discharges is are prolonged, favoring the evacuation of residents in the downstream area. The Peak-peak discharges at in S1, Yilongduo, Jiawu, and Ang'na villages are similar for each scenario, they are ~4,000 m³/s in of Scenario A1, ~6,000 m³/s in of Scenario A2, and ~10,000 m³/s in of Scenario A3. Wa'na Wa'na, Qiangjiuci, and Bula villages have similar peak discharges, which are ~3,800 m³/s, ~5,000 m³/s, and ~8,000 m³/s for Scenarios A1, A2, and A3, respectively. Beginning with From Bula village, the peak discharges of each scenario decrease significantly towards the downstream. Taking Scenario A3 as an example, at Bula village, the peak discharge is 7,512 m³/s at Bula village; then it is gradually less than 6,000 m³/s, 4,000 m³/s, 3,000 m³/s, and 1,000 m³/s from at Haqing village, Dama village, Qiwxing village to Xinka village village, it becomes smaller than 6,000 m³/s, at Dama village, it drops below 4,000 m³/s, at Qiwxing village it drops below 3,000 m³/s, and at Xinka village it decreases to below 1,000 m³/s (Fig. 13). The flood flow velocity velocities of GLOFs varies vary dramatically from upstream to downstream. At village S1, the maximum velocities of with Scenarios A1, A2, and A3 are corresponding to maximum velocities of 8.9 m/s, 12.2 m/s, and 14.9 m/s, respectively, at village S1. At Dading village, the maximum flow velocity velocities of GLOFs in Scenarios A1, A2, and A3 are all is approximately 2m/s.



565 **Figure 12.** The potential threat of GLOFs to settlements and roads downstream under different ice avalanche and landslide scenarios (the background is the MapWorld image).

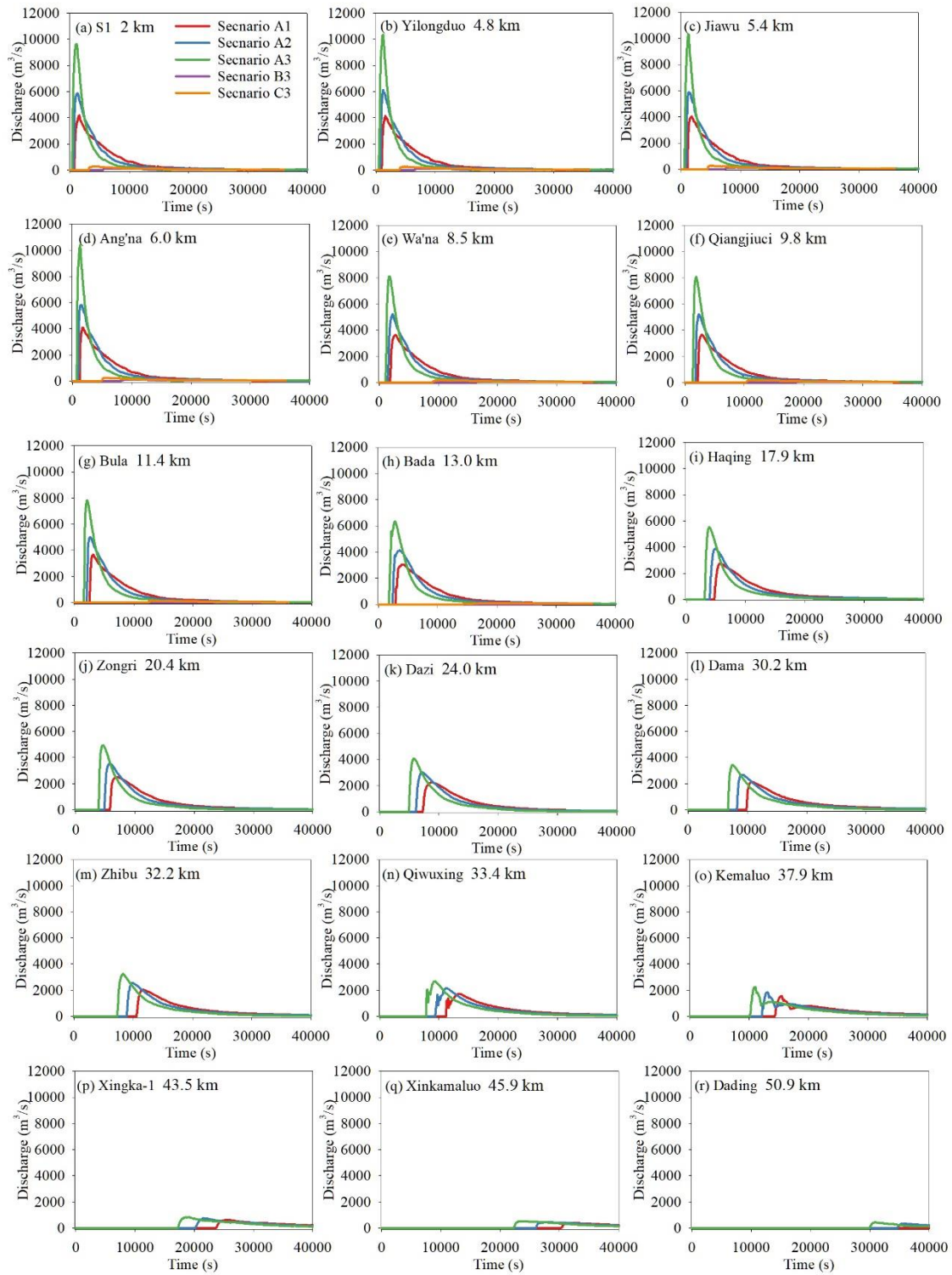
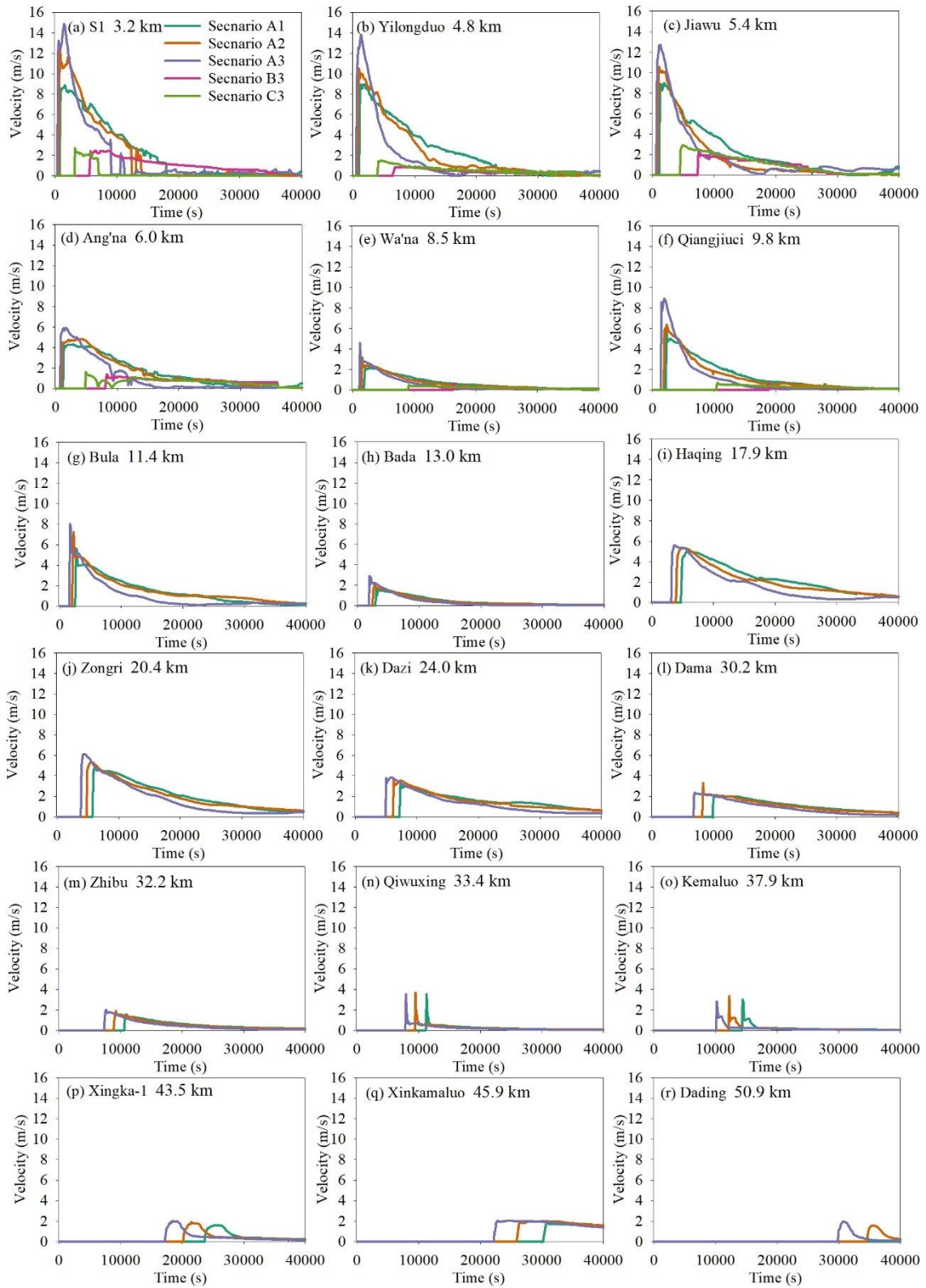


Figure 13. Time series of discharge at different settlements along the flow channel (locations in Fig. 1) of different scenarios.



570 **Figure 14.** Time series of velocity at different settlements along the flow channel (locations in Fig.1) of different scenarios.

5 Discussion

5.1 Lake volume of Bienong Co

Based on the accurate ~~bathymetric bathymetry results data of the~~from USV, we ~~found~~~~obtained~~ that the maximum and average depth of Bienong Co ~~were as~~ 181 m and 85.4 m ~~in August 2020~~, respectively, with ~~the a~~ lake volume of $102.3 \times 10^6 \text{ m}^3$. ~~in August 2020~~. Considering the rarity of ~~bathymetric bathymetry~~ data but the frequent ~~occurrence of~~ GLOFs in the Yi'ong Zangbo basin region, we attempted to ~~obtain~~~~explore~~ more information about glacial lakes in the region ~~by using~~~~from the~~ bathymetry ~~data and lake volume~~ of Bienong Co. First, relationships ~~with significant correlations~~ for area-volume, area-depth, and depth-volume of Bienong Co were established (Fig. 15), ~~and it~~ is hoped that this information could provide a valuable ~~data~~ reference for future studies of Bienong Co and other glacial lakes in the region. Then, we compared the depth and ~~lake~~ volume information of Bienong Co with other glacial lakes that have been measured. ~~At present~~, Bathymetry data are currently available for a small number of ~~there are few~~ glacial lakes ~~with measured bathymetry on~~ the Tibetan Plateau, ~~and they~~~~which~~ are mainly concentrated in the Himalayas of Nepal and the Poiqu ~~basin~~ Basin of Tibet, China. Longbasaba is a ~~n-end~~ moraine-dammed glacial lake located at the northern slope of the Himalayas, which had an area of $1.22 \pm 0.02 \text{ km}^2$ in 2009, with ~~an~~ average and maximum depths of $48 \pm 2 \text{ m}$ and $102 \pm 2 \text{ m}$, respectively, and a volume of $64 \times 10^6 \text{ m}^3$ (Yao et al., 2012). Although the area of Longbasaba is approximately 6% larger than that of Bienong Co, the ~~lake~~ volume is only 60% of that of Bienong Co. ~~This example shows that a glacial lake in the temperate glaciation zone is significantly larger in volume than a similarly sized glacial lake in the continental glaciation zone. However, due to the lack of measured bathymetric data of glacial lakes in the continental glaciation zone, no more comparisons can be made. We compared the depth and lake volume of Bienong Co with other glacial lakes in the temperate glaciation zone. The area of Luge glacial lake in Bhutan had was an area of approximately 1.17 km² in 2004, corresponding to the maximum and average depth of 49.8 m and 126 m, respectively, and an volume of $58 \times 10^6 \text{ m}^3$ (Yamada, 2004). in 2004, which~~ The area of Luge glacial lake is slightly larger than that of Bienong Co, ~~but~~ ~~the~~its average depth and maximum depth ~~were~~ 49.8 m and 126 m, respectively, with a lake volume of $58 \times 10^6 \text{ m}^3$ (Yamada, 2004), ~~which was~~is smaller than the corresponding values of Bienong Co. At the time of bathymetry, both South Lhonak lake in India and Imja glacial lake in Nepal had an area of approximately 1.3 km^2 , which is approximately 13% larger than that of Bienong Co, but both lakes have 64% and 76% of Bienong Co's volume, respectively (Sharma et al., 2018; Haritashya et al., 2018). Areas of Raphsthren glacial lake in Bhutan and Tsho Rolpa glacial lake in Nepal were 1.4 km^2 and 1.5 km^2 when bathymetries were carried out (Geological Survey of India, 1995; ICIMOD, 2011), which are 22% and 30% larger than that of Bienong Co, but their lake volumes ~~is are~~ 65% and 84% of that of Bienong Co, respectively. (Geological Survey of India, 1995; ICIMOD, 2011). The area of Lower Barun glacial lake in Nepal was 1.8 km^2 ~~when it was measured~~ (Haritashya et al., 2018), which is 57% larger than that of Bienong Co, ~~but~~ ~~However~~, the ~~lake~~ volume ~~was~~ ($112 \times 10^6 \text{ m}^3$), ~~which~~ is only 9% larger than that of Bienong Co (Haritashya et al., 2018), showing that Bienong Co is deeper ~~for~~in a same area. ~~and has larger volume.~~

Additionally, due to the scarcity of glacial lake bathymetry data and ~~its~~their importance ~~significance~~ for glacial lake GLOF hazard studies, scholars have proposed relationships to estimate ~~volumes of~~ glacial lakes ~~volumes through~~ ~~by~~ area, width, and length (O'Connor O'Connor et al., 2001; Huggel et al., 2002; Sakai, 2012; Wang et al., 2012a; Yao ~~er~~ et al., 2012; Cook and Quincey, 2015; Qi et al., 2022). We estimate the lake volume of Bienong Co using published ~~relationships~~equations based on glacial lakes on the Tibetan Plateau, ~~and~~ ~~it~~ The results show that the eight published volume-area/width-length relationships all underestimate the volume of Bienong Co to varying degrees. It can be inferred that Bienong Co is the ~~relative~~ deepest glacial lake in a same surface area among the glacial lakes with bathymetry data on the Tibetan Plateau. ~~among these on the Tibetan Plateau that currently have been measured. Whether this is unique to Bienong Co or a common feature of glacial lakes in the region is not yet known, as few glacial lakes in this region have field bathymetry. Future bathymetry is necessary~~

for more typical glacial lakes in the region.

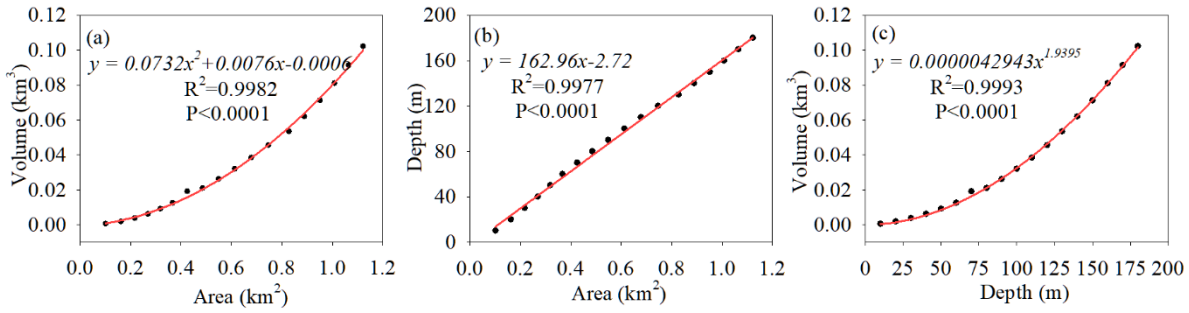


Figure 15. Fitting relationship of (a) area and volume, (b) area and depth and (c) depth and volume of Bienong Co.

Table 1. Calculated volumes of Bienong Co based on published volume-area relationships for glacial lakes in the Tibetan Plateau.

No	Source	Relationships	Calculated Volume	Error (%)
1	Qi et al., (2022)	(1) $V=0.04066A^{1.184}-0.003207w_{mx}/l_{mx}$	$46.9 \times 10^6 \text{ m}^3$	-54%
2		(2) $V=0.0126A^2+0.0056A+0.0132$	$36.3 \times 10^6 \text{ m}^3$	-65%
3	Wang et al., (2012)	$V=0.0354A^{1.3724}$	$42.9 \times 10^6 \text{ m}^3$	-58%
4	Sakai (2012)	$V=0.04324A^{1.5307}$	$53.6 \times 10^6 \text{ m}^3$	-48%
5	Yao et al., (2012)	$V=0.0493A^{0.9304}$	$56.1 \times 10^6 \text{ m}^3$	-45%
6	Fujita et al., (2013)	$V = 0.055A^{1.25}$	$65.5 \times 10^6 \text{ m}^3$	-36%
7	Khanal et al., (2015)	$V = 0.0578A^{1.5}$	$71.3 \times 10^6 \text{ m}^3$	-30%
8	Zhou et al., (2020)	$V=0.0717 w_{mx}^2 l_{mx}$	$70.3 \times 10^6 \text{ m}^3$	-31%

Note: Error = (volume of empirical formulas – bathymetrically-derived volume) / bathymetrically-derived volume × 100%.

5.2 Modelling explanation

The GLOF process chain simulated in this study starts with triggers, including ice avalanches from the mother glacier and landslides from the lateral moraines. Other triggers are not considered, such as increased glacial meltwater and heavy precipitation. Triggers are the beginning of the simulated GLOFs process chain in this study, and we only consider ice avalanche and landslide scenarios, instead of other factors, such as increased glacial meltwater and heavy precipitation. The magnitude, location, and probability of ice avalanches and landslides constitute are the this study's largest most significant uncertainty sources of uncertainty in this study. Ice avalanches are the triggered for over more than 70% of GLOFs on the Tibetan Plateau, but there is no reliable reference data for on the magnitude, including the release area and depth, of from previous ice avalanche events are scarce. Ice avalanches in this study come from the mother glacier tongue, where the slope is relatively steep and the fissures are well-developed. We simulated three different-magnitude ice avalanches, and each scenario assumes that the ice body breaks off in the vertical direction until it reaches the lake surface, which is unrealistic and may overestimate the volume of the ice avalanche. The RAMMS model can estimate the possible release volume based on the input DEM data, and the release area and, as well as the release depth, with t. The estimated released volume of Scenarios A1, A2, and A3 is $5 \times 10^6 \text{ m}^3$, $13.1 \times 10^6 \text{ m}^3$, and $41.3 \times 10^6 \text{ m}^3$ for Scenarios A1, A2, and A3, respectively. However, simulations show that approximately 76% ($3.8 \times 10^6 \text{ m}^3$), 37% ($4.9 \times 10^6 \text{ m}^3$), and 14% ($5.8 \times 10^6 \text{ m}^3$) of the estimated release volume enter the lake in Scenarios A1, A2, and A3, respectively. The simulation duration is set to 600 s to ensure the integrity of the ice avalanche process, with most of the ice body and most of the ice avalanche has already entered entering the lake within the first 100 s. The difference between the volume of the ice avalanche entering the lake and the estimated release volume is mainly determined by the slope and distance between the released ice body sources and the lake and the distance from the lake. In

640 Scenarios A2 and A3, the ice body entering the lake accounts for little of the estimated release volume due to a gentler slope and far distance between the released source and the lake. The gentler slope and far distance from the lake of the ice body in Scenarios A2 and A3 result in fewer ice avalanches entering the glacial lake, and The ice avalanche affect the process of ice avalanche material entering the lake is also affected, e.g., for example, Scenarios A2 and A3 fluctuated more dramatically have stronger fluctuations in the ice avalanche process than Scenario A1. In addition, we also consider landslides are determined as a trigger, given the failure of Jinwu Co in 2020. We selected Two two release areas release areas were selected by referring to the slope and location of Jinwu Co's landslide. However, the release depth has no specifically quantified reference. data and we We assumed three release depths of 2 m, 5 m, and 10 m for each release area for the to simulate multiple scenarios the consequences resulting from as many scenarios as possible.

645 In this study, A a reliable simulation of potentially future disaster-causing events, such as ice avalanches or landslides, in the future using scientific methods can assist people in understanding the possible risks and raise prevention awareness. However, accurate prediction is generally difficult due to limited geological information and details of triggering mechanisms such as extreme rainfall event. In this study, the RAMMS model was used to simulate the movements estimate the consequences of potential ice avalanches and landslides events. The accuracy and resolution of DEM data is crucial for the calculation of this the model, calculations, which can significantly greatly affect the paths, precision, and processes of mass movements topography and the avalanche and landslide pathways, and is concerned with the accurate reflection of the process of an ice avalanche event (Schneider et al., 2010). The accuracy of DEM is mainly related to two aspects. One is The issue of DEM accuracy in glacial environments is mainly due to the topographic changes of the glacial environment that occurs in the period between the times of the DEM data acquisition and the avalanche event. The other is the spatial resolution of DEM, with lower resolution one can lead to an overestimation of sediment area and an underestimation of sediment thickness (Cesca and D'Agostino, 2008). The ALOS PALSAR DEM data product used in this study was released globally in October 2014, with a spatial resolution of 12.5 m, which can generally reflect the intensity and pathway of the ice avalanches and landslides events simulated in this study. The volumes of future ice avalanches or landslides will almost certainly be smaller than the volumes formulated in this study due to glacier melting caused by climate warming. Moreover, the dry-Coulomb type friction μ and the viscous-turbulent friction ζ can also influence on the modelling results (Bezák et al., 2019). Mikoš and Bezák (2021) suggested found that the magnitude of mass movement ice avalanche or landslide magnitude slightly decreases and increases with increasing friction parameters μ and ζ , respectively, while the correlation is not strong. Schneider et al. (2014) found that a higher μ and ζ combinations leads to a higher peak velocities, faster stopping mechanisms, and hence shorter process durations. The values of μ and ζ cover wide ranges in the past applications (Mikoš and Bezák, 2021), and they were usually calibrated by actual events. In this study, We we chose the values of 0.12 and 1,000 m s⁻² as the values of for μ and ζ in this study, which were used in the avalanche simulation of Lake 513 (Schneider et al., 2014).

650 The BASEMENT model was applied to simulate the subsequent the GLOF process chains of GLOF process following ice avalanches and landslides. Much of the work on the generation, propagation and run-up of impulse wave has been focused on empirical models that replicate wave characteristics based on laboratory observations (Heller and Hager, 2010). Numerical simulations have been limited to simplified 2D SWEs simulations (Ghozlani et al., 2013), however However, the 2D SWEs are do not perform very well in avalanche-generated adequate to simulate waves simulations generated by avalanches because of the large energy dissipation due to caused by significant vertical accelerations (Lala et al., 2018). Therefore, empirical models are often used to calibrate the numerical simulations, for examples such as the Heller-Hager modeling result was employed to calibrate the simulation of the BASEMENT model in past studies (Byers et al., 2018; Lala et al., 2018). Nevertheless, the numerous parameters required by the Heller-Hager model are still subject to potential uncertainties because most of them are simple quantifications of the lake's geometry, owing to its simple quantifications about the geometry of the lake. Additionally, It is also mentioning that the BASEMENT model can only accept inflow in the form of water volume, but not actual the mass itself, such as the moraines, ice, snow, and mixtures their combinations (Kafle et al., 2016). Therefore, the actual situation of

680 ~~avalanches mixing with lake water cannot be simulated because the energy dissipation of water and avalanche entering the lake is different (Somos-Valenzuela et al., 2016).~~ Generally, simulations are calibrated by controlling the height and depth of the release area and converting the density between the material and water to influence the flow height and flow velocity in the model as avalanches enter a lake. However, the energy dissipation between the water and the true avalanche mixture is different, and the model can't present the real situation of the avalanche fluid mixing with a lake (Somos-Valenzuela et al., 685 ~~2016).~~ Furthermore, the maximum area of TIN representing a lake ~~also has slightly influences on the wave amplitude, smaller areas lead to finer values, which have little influence on the absolute value of wave amplitude.~~ The grain size distribution of Bienong Co's a moraine dam is ~~critical to its erosion simulation. an important parameter in simulating the moraine dam's erosions, but it is not obtained in this study. The S~~In this study, simulations were performed by referencing an inventory of the ~~grain size distribution~~ of glacial lakes in the Indian Himalayas. ~~The inventory that have has~~ been validated as generally reliable (Worni et al., 2013), but ~~the errors in Bienong Co are is~~ inevitable.

The ALOS PALSAR DEM ~~with a spatial resolution of 12.5 m~~ has been widely used in studies on cryospheric changes and disasters. ~~In this study, It the preprocessing of sink filling for the DEM was performed, pre-processed to fill sinks in this study, but there is still~~ the phenomenon of flood water accumulating in deep puddles ~~still exists,~~ especially in ~~the~~ relatively narrow valleys. We manually smoothed several large bumps according to the elevation of the upstream and downstream. 695 However, there are still some smaller bumps that converge the floodw to ~~some a section areas~~ of the flow channel, mainly in the downstream ~~area region~~. Therefore, the ~~GLOF impact flooding situation~~ in Qiwuxing, Kemaluo, Xingka, and Dading villages might be overestimated, especially in the former two villages because they are relatively far away from the river. The latter two villages are still very likely to be threatened by ~~flooding GLOFs~~ due to their proximity to the river. ~~More accurate simulations of GLOFs in the flow channel is limited by the~~ The resolution of ~~the~~ ALOS PALSAR DEM ~~is clearly insufficient for accurate simulation of flooding in the river channel.~~ Therefore, more precise topographic ~~information data,~~ such as DEM ~~data~~ generated from panchromatic stereo images with spatial resolutions better than 0.8 m obtained by the Gaofen-7 satellite and UAV-derived DEM products with low-cost are prospective. The frictional resistance in the downstream flow channel of Bienong Co is derived from the GLC10 LULC data, which basically fits the reality and has litter error of the simulations. GLOF flow processes can be very complex (Zhou et al., 2019), and flows can transform from clear water flow to hyper- 700 concentrated flow and then to debris flow, and these rheological transformations can occur in both space and time as the flow evolves (Worni et al., 2014). In this study, we do not consider the effects of sediment on flow rheology, ~~as well as and~~ the erosion and deposition of sediment along the flow path.

Emmer et al. (2022) divided the research evolution of GLOF process chains simulations into three stages, and this study belongs to the second stage, i.e., applying tailored physically based simulation tools for each component of the process chain and coupling them at the process boundaries. The third stage is the two-phase (Pudasaini, 2012) and three-phase (Pudasaini and Mergili, 2019) mass flow models and related simulation tools (Mergili et al., 2017; Mergili and Pudasaini, 2021) and the integrated simulations of the entire GLOF process chain in one single simulation step. The main advantage of the methods in the second stage is the simplicity and operability, with the convenient GUI interface of software in different links. Models for different links have been matured and widely applied in ~~the~~ corresponding fields with reliable performance and accessibility 710 of the required parameters. However, the third stage is undoubtedly the focus of future research to investigate the whole GLOF flooding process with more detail, in-depth, and better to reduce uncertainty in the coupling between different models. This will certainly involve more detailed parameters, increasing the difficulty of the simulation.

6 Conclusion

As a moraine-dammed glacial lake located in ~~a temperate glaciation region~~ the SETP, Bienong Co has been highly ~~focused on~~ ~~regarded~~ by local government due to its larger area and ~~the~~ high potential for GLOF hazards. Based on ~~bathymetric~~ ~~bathymetry~~

data, remote sensing images and DEM data, combined with ~~the~~ multiple models of RAMMS, BASEMENT, and Heller-Hager, we completed a comprehensive investigation of the potential GLOF process chain of Bienong Co, including ~~the~~ initial mass movements ~~s~~ from the mother glacier and the lateral moraines ~~s~~ ~~slope~~, displacement waves' generation and propagation in the lake, overtopping flows ~~s~~ and erosion on the moraine dam, and subsequent downstream ~~flooding~~ ~~floods~~. The following main results were obtained:

- (1) According to the ~~field bathymetric~~ ~~bathymetry~~ data, the ~~morphology of Bienong Co's~~ lake basin ~~morphology of Bienong Co~~ features a relatively flat ~~basin~~ bottom and steep flanks, with the slope near the glacier (16.5°) being steeper than that near the moraine dam (11.3°). The ~~water storage~~ ~~lake volume~~ of Bienong Co was $\sim 102.3 \times 10^6 \text{ m}^3$ in August 2020, with a maximum depth of $\sim 181 \text{ m}$. ~~Bienong Co is highly prone to a potential GLOF due to the~~ ~~The huge lake volume,~~ ~~enormous water storage combined with~~ the fissure-developed mother glacier tongue, steep ~~slope of~~ lateral moraines ~~slope~~, steep distal facing slope of the moraine dam, and low freeboard ~~make it possess high GLOF potential~~.
- (2) The volume of ~~materials~~ ~~mass~~ entering the lake for the three scenarios of ice avalanches (A1, A2, and A3) is much larger than that of the six scenarios of landslides (B1, B2, and B3 and C1, C2, and C3). Volumes of ice avalanches entering the lake in Scenarios A1, A2, and A3 are $3.8 \times 10^6 \text{ m}^3$, $4.9 \times 10^6 \text{ m}^3$, and $5.8 \times 10^6 \text{ m}^3$, respectively. Among the six landslide scenarios, Scenario B1 releases ~~a~~ ~~the~~ minimum volume of $0.03 \times 10^6 \text{ m}^3$, and Scenario C3 releases ~~a~~ ~~the~~ maximum volume of $0.30 \times 10^6 \text{ m}^3$. As a result, the impact zone, maximum flow height, and maximum flow ~~velocity of Scenarios A1, A2, and A3~~ ~~velocity~~ in the lake ~~also show that Scenarios A1, A2, and A3~~ are significantly larger than ~~those of Scenarios B1-3 and C1-3.~~ ~~the other six scenarios, in which Scenario B1 is the smallest and Scenario A3 is the largest.~~ Wave amplitudes near the moraine dam in Scenarios A1, A2, and A3 are 17.1 m, 20.2 m, and 25.2 m, respectively. ~~The~~ ~~o~~ Overtopping flows ~~s~~ of all three scenarios causes ~~dam~~ erosion ~~of the dam~~, with little difference in breach depth (19.0 m, 19.1 m, and 19.3 m), but ~~the~~ ~~larger~~ difference in breach width (295.0 m, 339.4 m, and 368.5 m). The volumes of water lost in the lake of ~~the three scenarios~~ ~~Scenarios A1, A2, and A3~~ are $24.1 \times 10^6 \text{ m}^3$, $25.3 \times 10^6 \text{ m}^3$, and $26.4 \times 10^6 \text{ m}^3$, ~~with~~ ~~and~~ ~~the~~ ~~flow~~ ~~peak~~ ~~flows~~ ~~discharges of~~ ~~are~~ 4,996 m^3/s , 7,817 m^3/s , and 13,078 m^3/s , respectively. Among ~~Scenarios B1-3 and C1-3~~ ~~the other six scenarios~~, only Scenarios B3 and C3 with larger magnitudes ~~cause dam erosion~~ ~~formed breaches on the moraine dam~~, with breach ~~depth~~ ~~es~~ of 6.5 m and 7.9 m ~~in depth~~ and ~~breach width of~~ 153 m and 169 m ~~in width~~, respectively.
- (3) ~~Floods~~ ~~GLOFs~~ all pass through 18 settlements in the downstream ~~river~~ ~~flow channel~~ in 20 h, with inundation areas of 7.6 km^2 , 8.0 km^2 , and 8.5 km^2 , ~~as well as~~ ~~and~~ average water depths of 8.4 m, 9.1 m, and 10.0 m, respectively. ~~The~~ GLOFs threatened ~~ed~~ more than half of the villages in the downstream ~~region~~ ~~flow channel~~. Scenarios B1, ~~and~~ B2, ~~and~~ C1, and C2 produce ~~very~~ limited overtopping flow that cannot poses a threat to the downstream ~~region~~ ~~settlements~~. Both Scenarios B3 and C3 produced ~~ed~~ ~~floods~~ ~~GLOFs~~ that flow through eight downstream settlements ~~within 20 h,~~ ~~and~~ ~~but~~ ~~the~~ ~~impact~~ ~~is~~ ~~had~~ ~~a~~ relatively small ~~impact on them~~.
- (4) Bienong Co is the ~~relative~~ ~~known~~ deepest glacial lake ~~among those~~ on the Tibetan Plateau ~~in the same surface area~~. ~~There are uncertainties in the GLOF process chain simulation in this study. However, it is significant for understanding the potential hazard of Bienong Co.~~ ~~that have currently been measured and is markedly different from glacial lakes on the south slope of the Himalayas.~~ ~~Furthermore, it is also important to use high precision topographic data for disaster simulation of GLOF lakes.~~

Code and data availability. The Landsat MSS/TM/OLI image are available from the United States Geological Survey (<https://earthexplorer.usgs.gov/>). The AST14DEM dataset and ALOS PALSAR DEM used in this study can be obtained from the National Aeronautics and Space Administration (NASA) EARTHDATA website (<https://earthdata.nasa.gov/>). The MapWorld image is provided by the National Platform for Common Geospatial Information Services (<https://www.tianditu.gov.cn/>). The GLC10 LULC product is available from http://data.ess.tsinghua.edu.cn/fromglc10_2017v01.html.

Author contributions. HD contributed the conceptualization, methodology, software, formal analysis, visualization and writing of the original draft; XY contributed the conceptualization, supervision, funding acquisition, investigation of the glacial lake, as well as review and editing of the manuscript; YZ, HJ, and QW contributed the investigation of the glacial lake; ZD, BW and QW contributed the model progress; JH contributed the setting up the experimental equipment and obtaining data.

Competing interests. The authors declare that they have no conflict of interest.

Financial support. This research has been supported by the National Key Research Program of China (grant no. 2019YFE0127700), the National Natural Science Foundation of China (grant nos. 41861013 and 42071089), "Innovation Star" of the Outstanding Graduate Student Program in Gansu Province (grant no. 2021-CXZX-215), Northwest Normal University's 2020 Graduate Research Grant Program (grant no. 2020KYZZ001012), and the Outstanding PhD Student Program in Gansu Province (grant no. 22JR5RA139).

References

~~Bartelt, P., Buehler, Y., Christen, M., Deubelbeiss, Y., Graf, C., McArdell, B., Sals, M., and Schneider, M.: RAMMS: Rapid mass movement simulation: a numerical model for debris flows in research and practice, User Manual v1.5—Debris Flow, Swiss Institute for Snow and Avalanche Research SLF, Birmensdorf, 2013.~~

Bezak, N., Sodnik, J., and Mikoš, M.: Impact of a random sequence of Debris flows on torrential fan formation, *Geosciences*, 9, 64, <https://doi.org/10.3390/geosciences9020064>, 2019.

Bolch, T., Peters, J., Yegorov, A., Pradhan, B., Buchroithner, M., and Blagoveshchensky, V.: Identification of potentially dangerous glacial lakes in the northern Tien Shan, *Nat. Hazards*, 59, 3, 1691–1714, <https://doi.org/10.1007/s11069-011-9860-2>, 2011.

Byers, A. C., Rounce, D. R., and Shugar, D. H.: A rockfall-induced glacial lake outburst flood, Upper Barun Valley, Nepal, *Landslides*, 16, 533–549, <https://doi.org/10.1007/s10346-018-1079-916>, 2018.

Byers, A. C., Chand, M. B., and Lala, J.: Reconstructing the history of glacial lake outburst floods (GLOF) in the Kanchenjunga conservation area, east Nepal: an interdisciplinary approach, *Sustainability*, 12, 5407, <https://doi.org/10.3390/su12135407>, 2020.

Brun, F., Berthier, E., Wagnon, P., Kääb, A., and Treichler, D.: A spatially resolved estimate of High Mountain Asia glacier mass balances from 2000 to 2016, *Nat. Geosci.*, 10, 668–673, <https://doi.org/10.1038/ngeo2999>, 2017.

Carrivick, J. L. and Tweed, F. S.: A global assessment of the societal impacts of glacier outburst floods, *Global. Planet. Change.*, 144, 1–16, <https://doi.org/10.1016/j.gloplacha.2016.07.001>, 2016.

Cesca, M. and D'Agostino, V.: Comparison between FLO-2D and RAMMS in debris-flow modelling: a case study in the Dolomites, *WIT Trans. Eng. Sci.*, 60, 197–206, <https://doi.org/10.2495/DEB080201>, 2008.

Cheng, Z. L., Zhu, P., Dang, C., and Liu, J. J.: Hazards of debris flow due to glacier lake outburst in Southeastern Tibet, *Journal of Glaciology and Geocryology*, 30, 954–959, <https://doi.org/CNKI:SUN:BCDT.0.2008-06-006>, 2008.

Cheng, Z. L., Liu, J. J., and Liu, J. K.: Debris flow induced by glacial-lake break in Southeast Tibet, *Earth Science Frontiers*, 16, 207–214, <https://doi.org/10.2495/DEB100091>, 2009.

~~Christen, M., Kowalski, J., and Bartelt, P.: RAMMS: numerical simulation of dense snow avalanches in three dimensional terrain, *Cold Reg. Sci. Technol.*, 63, 1–14, <https://doi.org/10.1016/j.coldregions.2010.04.005>, 2010.~~

Cook, S. J. and Quincey, D. J.: Estimating the volume of Alpine glacial lakes, *Earth. Surf. Dynam.*, 3, 559–575, <https://doi.org/10.5194/esurf-3-559-2015>, 2015.

Cook, K. L., Andermann, C., Gimbert, F., Adhikari, B. R., and Hovius, N.: Glacial lake outburst floods as drivers of fluvial erosion in the Himalaya, *Science*, 362, 53–57, <https://doi.org/10.1126/science.aat4981>, 2018.

- Coon, W. F.: Estimation of roughness coefficients for natural stream channels with vegetated banks, United States Geological Survey water-supply paper, 2441, 1998.
- 805 Cui, P., Ma, D. T., and Chen, N. S.: The initiation, motion and mitigation of debris flow caused by glacial lake outburst, *Quaternary Sciences*, 23, 621–628, [https://doi.org/10.1016/S0955-2219\(02\)00073-0](https://doi.org/10.1016/S0955-2219(02)00073-0), 2003.
- Dehecq, A., Gourmelen, N., Gardner, A. S., Brun, F., Goldberg, D., Nienow, P. W., Berthier, E., Vincent, C., Wagnon, P., and Trouvé, E.: Twenty-first century glacier slowdown driven by mass loss in High Mountain Asia, *Nat. Geosci.*, 12, 22–27, <https://doi.org/10.1038/s41561-018-0271-9>, 2019.
- 810 Duan, H. Y., Yao, X. J., Zhang, D. H., Qi, M. M., and Liu, J.: Glacial lake changes and identification of potentially dangerous glacial lakes in the Yi'ong Zangbo River Basin, *Water-Sui*, 12, 538, <https://doi.org/10.3390/w12020538>, 2020.
- Emmer, A. and Cochachin, A.: The causes and mechanisms of moraine-dammed lake failures in the Cordillera Blanca, North American Cordillera and Himalaya, *AUC. Geogr.*, 48, 5–15, <https://doi.org/10.14712/23361980.2014.23>, 2013.
- Emmer, A. and Vilimek, V.: New method for assessing the susceptibility of glacial lakes to outburst floods in the Cordillera Blanca, Peru, *Hydrol. Earth Syst. Sci.*, 18, 3461–3479, <https://doi.org/10.5194/hess-18-3461-2014>, 2014.
- 815 Emmer, A., Allen, S. K., Carey, M., Frey, H., Huggel, C., Korup, O., Mergili, M., Sattar, A., Veh, G., Chen, T. Y., Cook, S. J., Correias-Gonzalez, M., Das, S., Diaz Moreno, A., Drenkhan, F., Fischer, M., Immerzeel, W. W., Izagirre, E., Joshi, R. C., Kougkoulos, I., Knapp, R. K., Li, D. F., Majeed, U., Matti, S., Moulton, H., Nick, F., Piroton, V., Rashid, I., Reza, M., Figueiredo, A. R., Riveros, C., Shrestha, F., Shrestha, M., Steiner, J., Walker-Crawford, N., L. Wood, J., and Yde, J. C.: Progress and challenges in glacial lake outburst flood research (2017–2021): a research community perspective, *Nat. Hazards Earth Syst. Sci.*, 22, 3041–3061, <https://doi.org/10.5194/nhess-22-3041-2022>, 2022.
- 820 Evans, S. G.: The maximum discharge of outburst floods caused by the breaching of man-made and natural dams, *Can. Geotech. J.*, 24, 385–387, <https://doi.org/10.1139/t87-062>, 1987.
- Fujita, K., Sakai, A., Takenaka, S., Nuimura, T., Surazakov, A. B., Sawagaki, T., and Yamanokuchi, T.: Potential flood volume of Himalayan glacial lakes, *Nat. Hazards Earth Syst. Sci.*, 13, 1827–1839, <https://doi.org/10.5194/nhess-13-1827-2013>, 2013.
- 825 Geological Survey of India: Geology environmental hazards and remedial measures of the Lunana Area, Gasa Dzongkhong, Report of 1995 Indo-Bhutan Expedition, Bhutan Unit, Geological Survey of India, Samtse, 1995.
- Ghozlani, B., Zouhaier, H., and Khelifa, M.: Numerical study of surface water waves generated by mass movement, *Fluid Dyn. Res.*, 45, 055506, <https://doi.org/10.1088/0169-5983/45/5/055506>, 2013.
- 830 Haeberli, W., Käab, A., Vonder Mühl, D., and Teyssie, P.: Prevention of outburst floods from periglacial lakes at Grubengletscher, Valais, Swiss Alps, *J. Glaciol.*, 47, 111–122, <https://doi.org/10.3189/172756501781832575>, 2001.
- Haritashya, U. K., Kargel, J. S., Shugar, D. H., Leonard, G. J., Stratman, K., Watson, C. S., Shean, D., Harrison, S., Mandli, K. T., and Regmi, D.: Evolution and controls of large glacial lakes in the Nepal Himalaya, *Remote Sens-Basel*, 10, 798, <https://doi.org/10.3390/rs10050798>, 2018.
- 835 Harrison, S., Kargel, J. S., Huggel, C., Reynolds, J., Shugar, D. H., Betts, R. A., Emmer, A., Glasser, N., Haritashya, U. K., Klimeš, J., and Reinhardt, L.: Climate change and the global pattern of moraine-dammed glacial lake outburst floods, *The Cryosphere*, 12, 1195–1209, <https://doi.org/10.5194/tc-12-1195-2018>, 2018.
- Heller, V., Hager, W., and Minor, H. E.: Landslide generated impulse waves in reservoirs: Basics and computation, *Laboratory of Hydraulics, Hydrology, and Glaciology, ETH Zürich, Switzerland*, 172, 2009.
- 840 Heller, V. and Hager, W. H.: Impulse product parameter in landslide generated impulse waves, *J. Waterw. Port. Coast.*, 136, 145–155, [https://doi.org/10.1061/\(ASCE\)WW.1943-5460.0000037](https://doi.org/10.1061/(ASCE)WW.1943-5460.0000037), 2010.
- Huang, L., Zhu, L. P., Wang, J. B., Ju, J. T., Wang, Y., Zhang, J. F., and Yang, R. M.: Glacial activity reflected in a continuous lacustrine record since the early Holocene from the proglacial Laigu Lake on the southeastern Tibetan Plateau, *Palaeogeogr. Palaeoclimatol.*, 456, 37–45, <https://doi.org/10.1016/j.palaeo.2016.05.019>, 2016.
- 845 Huggel, C., Käab, A., Haeberli, W., Teyssie, P., and Paul, F.: Remote sensing based assessment of hazards from glacier lake

- outbursts: a case study in the Swiss Alps, *Can. Geotech. J.*, 39, 316–330, <https://doi.org/10.1139/t01-099>, 2002.
- Huggel, C., Haeberli, W., Kääb, A., Bieri, D., and Richardson, S.: An assessment procedure for glacial hazards in the Swiss Alps, *Can. Geotech. J.*, 41, 1068–1083, <https://doi.org/10.1139/t04-053>, 2004.
- International Centre for Integrated Mountain Development (ICIMOD): Glacial lakes and glacial lake outburst floods in Nepal, ICIMOD, Kathmandu, 99, 2011.
- 850 Kafle, J., Pokhrel, P. R., Khattri, K. B., Kattel, P., Tuladhar, B. M., and Pudasain, S. P.: Landslide-generated tsunami and particle transport in mountain lakes and reservoirs, *Ann. Glaciol.*, 57, 232–244, doi: 10.3189/2016AoG71A034, 2016.
- Kääb, A., Berthier, E., Nuth, C., Gardelle, J., and Arnaud, Y.: Contrasting patterns of early twenty-first-century glacier mass change in the Himalayas, *Nature*, 488, 495–498, <https://doi.org/10.1038/nature11324>, 2012.
- 855 Kääb, A., Treichler, D., Nuth, C., and Berthier, E.: Brief communication: contending estimates of 2003–2008 glacier mass balance over the Pamir-Karakoram-Himalaya, *The Cryosphere*, 9, 557–564, <https://doi.org/10.5194/tc-9-557-2015>, 2015.
- Ke, C. Q., Kou, C., Ludwig, R., and Qin, X.: Glacier velocity measurements in the eastern Yigong Zangbo basin, Tibet, China, *J. Glaciol.*, 59, 1060–1068, <https://doi.org/10.3189/2013jog12j234>, 2013.
- Ke, C. Q., Han, Y. F., and Kou, C.: Glacier change in the Yigong Zangbu Basin, Tibet, China (1988 to 2010), *Dragon 3Mid*
- 860 *Term Results*, 724, <http://articles.adsabs.harvard.edu/pdf/2014ESASP.724E.16K>, 2014.
- Lala, J. M., Rounce, D. R., and Mckinney, D. C.: Modeling the glacial lake outburst flood process chain in the Nepal Himalaya: Reassessing Imja Tsho’s hazard, *Hydro. Earth. Syst. Sci.*, 22, 3721–3737, <https://doi.org/10.5194/hess-2017-683>, 2018.
- Larrazabal, J. M. and Peñas, M. S.: Intelligent rudder control of an unmanned surface vessel, *Expert. Syst. Appl.*, 55, 106–117, <https://doi.org/10.1016/j.eswa.2016.01.057>, 2016.
- 865 Li, J.J., Zhen, B. X., and Yang, X. J.: *Glaciers in Tibet*, Science Press, Beijing, 1986.
- Li, D., Shangguan D. H., Wang, X.Y., Ding, Y. J., Su, P. C., Liu, R. L., and Wang, M. X.: Expansion and hazard risk assessment of glacial lake Jialong Co in the central Himalayas by using an unmanned surface vessel and remote sensing, *Sci. Total. Environ.*, 784, 147249, <https://doi.org/10.1016/j.scitotenv.2021.147249>, 2021.
- LIGG/WECS/NEA: Report on first expedition to glaciers and glacier lakes in the Pumqu (Arun) and Poiqu (Bhote-Sun Koshi)
- 870 *River Basins, Xizang (Tibet), China, Sino-Nepalese Joint Investigation of Glacier Lake Outburst Flood in Himalayas in 1987*, 192, 1988.
- Liu, J. K., Zhou, L. X., Zhang, J. J., and Zhao, W. Y.: Characteristics of Jiwencuo GLOF, Lhari county, Tibet, *Geological Review*, 67: 17–18. <https://doi.org/10.16509/j.georeview.2021.s1.007>, 2021.
- Liu, S. Y., Pu, J. C., and Deng, X. F.: *Glaciers and glacier landscapes in China*, Shanghai Popular Science Press, Shanghai, 38–
- 875 41, 2014.
- Liu, W. M., Lai, Z. P., Hu, K. H., Ge, Y. G., Cui, P., Zhang, X. G., and Liu, F.: Age and extent of a giant glacial-dammed lake at Yarlung Tsangpo gorge in the Tibetan Plateau, *Geomorphology*, 246, 370–376, <https://doi.org/10.1016/j.geomorph.2015.06.034>, 2015.
- Liu, Z. X., Zhang, Y. M., Yu, X., and Yuan, C.: Unmanned surface vehicles: an overview of developments and challenges, *Annu. Rev. Control.*, 41, 71–39, <https://doi.org/10.1016/j.arcontrol.2016.04.018>, 2016.
- 880 Liu, J. k., Zhang, J. J., Gao, Bo., Li, Y. L., Li, M. Y., Wujin, D. J., and Zhou, L. X.: An overview of glacial lake outburst flood in Tibet, China, *Journal of Glaciology and Geocryology*, 41, 1335–1347, <https://doi.org/10.7522/j.issn.1000-0240.2019.0073>, 2019.
- Lliboutry, L.: Glaciological problems set by the control of dangerous lakes in Cordillera Blanca, Peru, II. Movement of a covered glacier embedded within a rock glacier, *J. Glaciol.*, 18, 255–274, <https://doi.org/10.3189/S0022143000021341>, 1977.
- Lv, R. R., Tang, X. B., and Li, D. J.: *Glacial lake outburst mudslide in Tibet*, Chengdu University of Science and Technology Press, Chengdu, 69–105, 1999.
- Mckillop, R. J. and Clague, J.: Statistical, remote sensing-based approach for estimating the probability of catastrophic

- drainage from moraine-dammed lakes in southwestern British Columbia, *Global Planet Change*, 56, 153–171, <https://doi.org/10.1016/J.GLOPLACHA.2006.07.004>, 2007.
- 890 Mergili, M. and Schneider, J. F.: Regional-scale analysis of lake outburst hazards in the southwestern Pamir, Tajikistan, based on remote sensing and GIS, *Nat. Hazards Earth Syst. Sci.*, 11, 1447–1462, <https://doi.org/10.5194/nhess-11-1447-2011>, 2011.
- Mergili, M., Fischer, J. T., Krenn, J., and Pudasaini, S. P.: r.avaflow v1, an advanced open-source computational framework for the propagation and interaction of two-phase mass flows, *Geosci. Model Dev.*, 10, 553–569, <https://doi.org/10.5194/gmd-10-553-2017>, 2017.
- 895 Mergili, M. and Pudasaini, S. P.: r.avaflow-The open source mass flow simulation model, <https://www.avaflow.org/>, last access: 1 October 2021.
- Mikoš, M. and Bezak, N.: Debris flow modelling using RAMMS model in the Alpine environment with focus on the model parameters and main characteristics, *Front. Earth Sci.* 8:605061. <https://doi.org/10.3389/feart.2020.605061>, 2021.
- 900 Mool, P. K., Bajracharya, S. R., and Joshi, S. P.: Inventory of glaciers, glacial lakes and glacial lake outburst floods, monitoring and early warning systems in the Hindu Kush- Himalayan region: Nepal, ICIMOD & UNEP RRC-AP, 363, 2001.
- Neckel, N., Kropáček, J., Bolch, T., and Hochschild, V.: Glacier mass changes on the Tibetan Plateau 2003-2009 derived from ICESat laser altimetry measurements, *Environ. Res. Lett.*, 9, 468–475, <https://doi.org/10.1088/1748-9326/9/1/014009>, 2014.
- Nie, Y., Liu, Q., Wang, J. D., Zhang, Y. L., Sheng, Y. W., and Liu, S. Y.: An inventory of historical glacial lake outburst floods in the Himalayas based on remote sensing observations and geo-morphological analysis, *Geomorphology*, 308, 91–106, <https://doi.org/10.1016/j.geomorph.2018.02.002>, 2018.
- 905 O’Connor, J. E., Hardison, J. H., and Costa, J. E.: Debris flows from failures of neoglacial-age moraine dams in the Three Sisters and Mount Jefferson wilderness areas, Oregon, United States Geological Survey Professional Paper, 1606, 11–40, <https://doi.org/10.1007/BF01211117>, 2001.
- 910 Osti, R. and Egashira, S.: Hydrodynamic characteristics of the Tam Pokhari glacial lake outburst flood in the Mt. Everest region, Nepal, *Hydrol. Process.*, 23, 2943–2955, <https://doi.org/10.1002/hyp.7405>, 2009.
- Prakash, C. and Nagarajan, R.: Outburst susceptibility assessment of moraine-dammed lakes in Western Himalaya using an analytic hierarchy process, *Earth. Surf. Proc. Land.*, 42, 2306–2321, <https://doi.org/10.1002/esp.4185>, 2017.
- Pudasaini, S. P.: A general two-phase debris flow model, *J. Geo-phys. Res.*, 117, F03010, <https://doi.org/10.1029/2011JF002186>, 2012.
- 915 Pudasaini, S. P. and Mergili, M.: A multi-phase mass flow model, *J. Geophys. Res-sol Ea*, 124, 2920–2942, <https://doi.org/10.1029/2019jf005204>, 2019.
- Qi, M. M., Liu, S. Y., Yao, X. J., Grünwald, R., and Liu, J.: Lake inventory and potentially dangerous glacial lakes in the Nyang Qu Basin of China between 1970 and 2016, *J. Mt. Sci-Engl*, 17, 851–870, <https://doi.org/10.1007/s11629-019-5675-5>, 2020.
- 920 Qin D. H., Dong, W. J., and Luo, Y.: Climate and environment change in China, China Meteorological Press, Beijing, 116-121, 2012.
- [RAMMS: AVALANCHE User Manual, v1.70, Switzerland: ETH, Available at: https://ramms.slf.ch/ramms/downloads/RAMMS_AVAL_Manual.pdf, 2017.](https://ramms.slf.ch/ramms/downloads/RAMMS_AVAL_Manual.pdf)
- Richardson, S. D. and Reynolds, J. M.: An overview of glacial hazards in the Himalayas, *Quatern. Int.*, 65, 31–47, [https://doi.org/10.1016/S1040-6182\(99\)00035-X](https://doi.org/10.1016/S1040-6182(99)00035-X), 2000.
- 925 Risio, M., Girolamo, P. D., and Beltrami, G. M.: Forecasting landslide generated Tsunamis: a review, the Tsunami threat-research and technology, 81–106, <https://doi.org/10.5772/13767>, 2011.
- Rounce, D. R., McKinney, D. C., Lala, J. M., Byers, A. C., and Watson, C. S.: A new remote hazard and risk assessment framework for glacial lakes in the Nepal Himalaya, *Hydrol. Earth Syst. Sci.*, 20, 3455–3475, <https://doi.org/10.5194/hess-20-3455-2016>, 2016.
- 930 Sakai, A., Yamada, T., and Fujita, K.: Volume change of Imja Glacial Lake in the Nepal Himalayas, International Symposium

- on Disaster Mitigation & Basin Wide Water Management, Niigata, 556–561. 2003.
- Sakai, A.: Glacial lakes in the Himalayas: a review on formation and expansion processes, *Global Environmental Research*, 16, 23–30, 2012.
- 935 Sattar, A., Goswami, A., and Kulkarni, A. V.: Hydrodynamic moraine-breach modeling and outburst flood routing - a hazard assessment of the South Lhonak lake, Sikkim, *Sci. Total. Environ.*, 668, 362–378, <https://doi.org/10.1016/j.scitotenv.2019.02.388>, 2019.
- Sattar, A., Haritashya, U. K., Kargel, J. S., Leonard, G. J., and Chase, D. V.: Modeling lake outburst and downstream hazard assessment of the Lower Barun Glacial Lake, Nepal Himalaya, *J. Hydrol.*, 598, 126208, <https://doi.org/10.1016/j.jhydrol.2021.126208>, 2021.
- 940 Schneider, D., Bartelt, P., Caplan-Auerbach, J., Christen, M., Huggel, C., and W. McArdeell, B.: Insights into rock-ice avalanche dynamics by combined analysis of seismic recordings and a numerical avalanche model, *J. Geophys. Res.*, 115, F04026, <https://doi.org/10.1029/2010JF001734>, 2010.
- Schneider, D., Huggel, C., Cochachin, A., Guillén, S., and García, J.: Mapping hazards from glacier lake outburst floods based on modelling of process cascades at Lake 513, Carhuaz, Peru, *Adv. Geosci*, 35, 145–155, <https://doi.org/10.5194/adgeo-35-145-2014>, 2014.
- 945 Sharma, R. K., Pradhan, P., Sharma, N. P., and Shrestha, D. G.: Remote sensing and in situ-based assessment of rapidly growing South Lhonak glacial lake in eastern Himalaya, India, *Nat. Hazards.*, 93, 393, <https://doi.org/10.1007/s11069-018-3348-2>, 2018.
- 950 Shi, W. L., Yang, C. T., You, G. X., and Jin, M. X.: The measurement of reserve of glacier block lake on the upper stream of Yerqiang river and the calculation of its maximum flood, *Arid Land Geography.*, 14, 31–35, 1991.
- Shugar, D., Burr, A., Haritashya, U. K., Kargel, J. S., Watson, C. S., Kennedy, M. C., Bevington, A. R., Betts, R. A., Harrison, S., and Stratman, K.: Rapid worldwide growth of glacial lakes since 1990, *Nat. Clim. Change.*, 10, 939–945, <https://doi.org/10.1038/s41558-020-0855-4>, 2020.
- 955 [Singh, V. P.: Dam Breach Modelling Technology, Kluwer Academic Publishers, Dordrecht, Boston, London, 1996.](#)
- Song, C. Q., Sheng, Y. W., Ke, L. H., Nie, Y., and Wang, J. D.: Glacial lake evolution in the southeastern Tibetan Plateau and the cause of rapid expansion of proglacial lakes linked to glacial-hydrogeomorphic processes, *J. Hydrol.*, 540, 504–514, <https://doi.org/10.1016/j.jhydrol.2016.06.054>, 2016.
- Somos-Valenzuela, M. A., Chisolm, R. E., Rivas, D. S., Portocarrero, C., and McKinney, D. C.: Modeling glacial lake outburst flood process chain: the case of Lake Palcacocha and Huaraz, Peru, *Hydrol. Earth Syst. Sci.*, 20, 2519–2543, <https://doi.org/10.5194/hess-2015-512>, 2016.
- 960 Specht, M., Specht, C., Lasota, H., and Cywiński, P.: Assessment of the steering precision of a hydrographic unmanned surface vessel (USV) along sounding profiles using a low-cost multi-global navigation satellite system (GNSS) receiver supported autopilot, *Sensors-Basel*, 19, 3939, <https://doi.org/10.3390/s19183939>, 2019.
- 965 Sun, M. P., Liu, S. Y., Yao, X. J., and Li, L.: The cause and potential hazard of glacial lake outburst flood occurred on July 5, 2013 in Jiali County, Tibet, *Journal of Glaciology and Geocryology*, 36, 158–165, <https://doi.org/158-165,10.7522/j.issn.1000-0240.2014.0020>, 2014.
- Thompson, S., Benn, D. I., Mertes, J., and Luckman, A.: Stagnation and mass loss on a Himalayan debris-covered glacier: Processes, patterns and rates, *J. Glaciol.*, 62, 467–485, <https://doi.org/10.1017/jog.2016.37>, 2016.
- 970 Veh, G., Korup, O., Specht, S. V., Roessner, S., and Walz, A.: Unchanged frequency of moraine-dammed glacial lake outburst floods in the Himalaya, *Nat. Clim. Change.*, 9, 379–383, <https://doi.org/10.1038/s41558-019-0437-5>, 2019.
- Vetsch, D., Siviglia, A., Bürgler, M., Caponi, F., Ehrbar, D., Facchini, M., Faeh, R., Farshi, D., Gerber, M., Gerke, E., Kammerer, S., Koch, A., Mueller, R., Peter, S., Rousselot, P., Vanzo, D., Veprek, R., Volz, C., Vonwiller, L., and Weberndorfer, M.: System manuals of BASEMENT, Version 2.8.2 Laboratory of Hydraulics, Glaciology and Hydrology (VAW). ETH Zurich. Available

- 975 from <http://www.basement.ethz.ch>. [3 October 2022].
- Vilímek, V., Emmer, A., Huggel, C., Schaub, Y., and Würmli, S.: Database of glacial lake outburst floods (GLOFs)-IPL project no. 179, *Landslides*, 11, 161–165, <https://doi.org/10.1007/s10346-013-0448-7>, 2013.
- Wang, S. J., Che, Y. J., and Ma, X. G.: Integrated risk assessment of glacier lake outburst flood (GLOF) disaster over the Qinghai-Tibetan Plateau (QTP), *Landslides*, 17, 2849–2863, <https://doi.org/10.1007/s10346-020-01443-1>, 2020b.
- 980 Wang, S. J., Yang, Y., Gong, W., Che, Y., Ma, X., and Xie, J.: Reason analysis of the Jiwenco glacial lake outburst flood (GLOF) and potential hazard on the Qinghai-Tibetan Plateau, *Remote Sens-Basel*, 13, 3114, <https://doi.org/10.3390/rs13163114>, 2021.
- [Wang, W. C., Yang, X. X., and Yao, T. D.: Evaluation of ASTER GDEM and SRTM and their suitability in hydraulic modelling of a glacial lake outburst flood in southeast Tibet, *Hydrol. Process.*, 26, 213–225, <https://doi.org/10.1002/hyp.8127>, 2011a.](#)
- Wang, W. C., Yao, T. D., Gao, Y., Yang, X. X., and Kattel, D. B.: A first-order method to identify potentially dangerous glacial lakes in a region of the southeastern Tibetan Plateau, *Mt. Res. Dev.*, 31, 122–130, <https://doi.org/10.1659/MRD-JOURNAL-D-10-00059.1>, [2011a](#)[2011b](#).
- [Wang, W. C., Yang, X. X., and Yao, T. D.: Evaluation of ASTER GDEM and SRTM and their suitability in hydraulic modelling of a glacial lake outburst flood in southeast Tibet, *Hydrol. Process.*, 26, 213–225, <https://doi.org/10.1002/hyp.8127>, 2011b.](#)
- Wang, W. C., Yao, T. D., Yang, W., Joswiak, D., and Zhu, M. L.: Methods for assessing regional glacial lake variation and hazard in the southeastern Tibetan Plateau: a case study from the Boshula mountain range, China, *Environ. Earth. Sci.*, 67, 1441–1450, <https://doi.org/10.1007/s12665-012-1589-z>, 2012.
- Wang, W. C., Gao, Y., Anaconda, P. I., Lei, Y. B., Xiang, Y., Zhang G. Q., Li, S. H., and Lu, A. X.: Integrated hazard assessment of Cirenmaco glacial lake in Zhangzangbo valley, Central Himalayas, *Geomorphology*, 306, 292–305, <https://doi.org/10.1016/j.geomorph.2015.08.013>, 2015.
- 995 Wang, X., Liu, S. Y., Guo, W. Q., Yao, X. J., Jiang, Z. L., and Han, Y. S.: Using remote sensing data to quantify changes in glacial lakes in the Chinese Himalaya, *Mt. Res. Dev.*, 32, 203–212, <https://doi.org/10.1659/MRD-JOURNAL-D-11-00044.1>, 2012a.
- Wang, X., Liu, S. Y., Ding, Y. J., Guo, W. Q., Jiang, Z. L., Lin, J., and Han, Y.: An approach for estimating the breach probabilities of moraine-dammed lakes in the Chinese Himalayas using remote-sensing data, *Nat. Hazards Earth Syst. Sci.*, 12, 3109–3122, <https://doi.org/10.5194/nhess-12-3109-2012>, 2012b.
- 1000 Wang, X.: Methodology and application of moraine lake outburst hazard evaluation in the Chinese Himalayas, Science Press, Beijing, 2016.
- Wang, X., Chai, K. G., Liu, S. Y., Wei, J. F., Jiang, Z. L., and Liu, Q. H.: Changes of glaciers and glacial lakes implying corridor-barrier effects and climate change in the Hengduan Shan, southeastern Tibetan Plateau, *J. Glaciology.*, 63, 535–542, <https://doi.org/10.1017/jog.2017.14>, 2017.
- 1005 Watanbe, T. and Rothacher, D.: The 1994 Lugge Tsho glacial lake outburst flood, Bhutan Himalaya, *Mt. Res. Dev.*, 16, 77–81, <https://doi.org/10.2307/3673897>, 1996.
- Watson, C. S., Quincey, D. J., Carrivick, J. L., Smith, M. W., Rowan, A. V., and Richardson, R.: Heterogeneous water storage and thermal regime of supraglacial ponds on debris covered glaciers, *Earth. Surf. Proc. Land.*, 43, 229–241, <https://doi.org/10.1002/esp.4236>, 2018.
- 1010 Westoby, M. J., Glasser, N. F., Brasington, J., Hambrey, M. J., Quincey, D. J., and Reynolds, J. M.: Modelling outburst floods from moraine-dammed glacial lakes, *Earth-Sci. Rev.*, 134, 137–159, <https://doi.org/10.1016/j.earscirev.2014.03.009>, 2014.
- Worni, R., Huggel, C., and Stoffel, M.: Glacial lakes in the Indian Himalayas - from an area-wide glacial lake inventory to an on-site and modeling based risk assessment of critical glacial lakes, *Sci. Total Environ*, 468, S71–S84, <https://doi.org/10.1016/j.scitotenv.2012.11.043>, 2013.
- 1015 Worni, R., Huggel, C., Clague, J. J., Schaub, Y., and Stoffel, M.: Coupling glacial lake impact, dam breach, and flood processes:

- A modeling perspective, *Geomorphology*, 224, 161–176, <https://doi.org/10.1016/j.geomorph.2014.06.031>, 2014.
- Wong, M. and Parker, G.: Reanalysis and correction of bed-load relation of meyer-peter and mä¹/₄ller using their own database, *Journal of Hydraulic Engineering*, 132, 1159–1168, <https://doi.org/10.1111/j.1600-0587.1978.tb00950.x>, 2006.
- 1020 Yan, R. J., Pang, S., Sun, H. B., and Pang, Y. J.: Development and missions of unmanned surface vehicle, *J. Mar. Sci. Appl.*, 9, 451–457, <https://doi.org/10.1007/s11804-010-1033-2>, 2010.
- Yang, W., Yao, T. D., Xu, B. Q., Wu, G. J., Ma, L. L., and Xin, X. D.: Quick ice mass loss and abrupt retreat of the maritime glaciers in the Kangri Karpo Mountains, southeast Tibetan Plateau, *Chin. Sci. Bull.*, 53, 2547–2551, <https://doi.org/10.1007/s11434-008-0288-3>, 2008.
- 1025 Yamada, T.: Glacier lake and its outburst flood in the Nepal Himalaya, Data Center for Glacier Research, Japanese Society of Snow and Ice, 1, 96, 1998.
- Yamada, T., Naito, N., Kohshima, S., Fushimi, H., Nakazawa, F., Segawa, T., Uetake, J., Suzuki, R., Sato, N., Karma, Chhetri, I. K., Gyenden, L., Yabuki, H., and Chikita, K.: Outline of 2002: research activity on glaciers and glacier lakes in Lunana region, Bhutan Himalayas, *Bull. Glaciol. Res.*, 21: 79–90, 2004.
- 1030 Yao, X. J., Liu, S. Y., Sun, M. P., Wei, J. F., and Guo, W. Q.: Volume calculation and analysis of the changes in moraine-dammed lakes in the north Himalaya: a case study of Longbasaba lake, *J. Glaciol.*, 58, 753–760, <https://doi.org/10.3189/2012JoG11J048>, 2012.
- Yao, X. J., Liu, S. Y., Sun, M. P., and Zhang, X. J.: Study on the glacial lake outburst flood events in Tibet since the 20th century, *Journal of Natural Resources*, 8, 1377–1390, <https://doi.org/10.11849/zrzyxb.2014.08.010>, 2014.
- 1035 Yuan, G. and Zeng, Q.: Glacier-dammed Lake in Southeastern Tibetan Plateau during the Last Glacial Maximum, *J. Geol. Soc. India.*, 79, 295–301, <https://doi.org/10.1007/s12594-012-0041-z>, 2012.
- Zemp, M., Huss, M., Thibert, E., Eckert, N., McNabb, R., Huber, J., Barandun, M., Machguth, H., Nussbaumer, S. U., Gartner-Roer, I., Thomson, L., Paul, F., Maussion, F., Kutuzov, S., and Cogley, J. G.: Global glacier mass changes and their contributions to sea-level rise from 1961 to 2016, *Nature*, 568, 382–386, <https://doi.org/10.1038/s41586-019-1071-0>, 2019.
- 1040 Zhang, B., Liu, G. X., Zhang, R., Fu, Y., and Li, Z. L.: Monitoring dynamic evolution of the glacial lakes by using time series of Sentinel-1A SAR images, *Remote Sens-Basel*, 13, 1313, <https://doi.org/10.3390/rs13071313>, 2021.
- Zhang, M. M., Chen, F., Tian, B. S., Liang, D., and Yang, A. Q.: High-frequency glacial lake mapping using time series of Sentinel-1A/1B SAR imagery: An assessment for southeastern Tibetan Plateau, *Nat. Hazard. Earth. Sys.*, 1–18, <https://doi.org/10.5194/nhess-2019-219>, 2020.
- 1045 Zhang, Y., Yao, X. J., Duan, H. Y., and Wang, Q.: Simulation of glacial lake outburst flood in Southeastern Qinghai-Tibet plateau - a case study of Jiwen Co Glacial Lake, *Frontiers in Earth Science*, 10: 1–13. <https://doi: 10.3389/feart.2022.819526>, 2022.
- Zhang, D. H., Zhou, G., Li, W., Han, L., Zhang, S., Yao, X. J., and Duan, H. Y.: A robust glacial lake outburst hazard assessment system validated by GLOF event in 2020 in the Nidu Zangbo Basin, Tibetan Plateau, *Catena*, 220, 106734, <https://doi.org/10.2139/ssrn.3962879>, 2023.
- 1050 Zheng, G. X., Mergili, M., Emmer, A., Allen, S., and Stoffel, M.: The 2020 glacial lake outburst flood at Jinwu Co, Tibet: causes, impacts, and implications for hazard and risk assessment, *The Cryosphere*, 15, 3159–3180, <https://doi.org/10.5194/tc-2020-379>, 2021.
- 1055 Zhou, G. G. D., Zhou, M. J., Shrestha, M. S., Song, D. R., Choi, C. E., Cui, K. F. E., Peng, M., Shi, Z. M., Zhu, X. H., and Chen, H. Y.: Experimental investigation on the longitudinal evolution of land- slide dam breaching and outburst floods, *Geomorphology* 334, 29–43, <https://doi.org/10.1016/j.geomorph.2019.02.035>, 2019.
- Zhou, L. X., Liu, J. K., and Li, Y. L.: Calculation method of mathematical model of the moraine dammed lake storage capacity, *Science Technology and Engineering*, 20, 9804–9809, 2020.
- 1060

